OXFORD

# Retention of stress susceptibility in the *mdx* mouse model of Duchenne muscular dystrophy after PGC-1α overexpression or ablation of IDO1 or CD38

Erynn E. Johnson [iD][1], W. Michael Southern[1], Baird Doud[1], Brandon Steiger[1], Maria Razzoli[2], Alessandro Bartolomucci[2],

James M. Ervasti[1,*]

[1]Department of Biochemistry, Molecular Biology, and Biophysics, University of Minnesota Medical School, 420 Delaware St. SE, Minneapolis, MN 55455, United States
[2]Department of Integrative Biology and Physiology, University of Minnesota Medical School, 321 Church St. SE, Minneapolis, MN 55455, United States
*Corresponding author. Department of Biochemistry, Molecular Biology, and Biophysics, University of Minnesota, Research Director, Paul and Sheila Wellstone Muscular Dystrophy Center, 6-155 Jackson Hall, 321 Church St SE, Minneapolis, MN 55455, United States. E-mail: jervasti@umn.edu

## Abstract

Duchenne muscular dystrophy (DMD) is a lethal degenerative muscle wasting disease caused by the loss of the structural protein dystrophin with secondary pathological manifestations including metabolic dysfunction, mood and behavioral disorders. In the mildly affected *mdx* mouse model of DMD, brief scruff stress causes inactivity, while more severe subordination stress results in lethality. Here, we investigated the kynurenine pathway of tryptophan degradation and the nicotinamide adenine dinucleotide ($NAD^+$) metabolic pathway in *mdx* mice and their involvement as possible mediators of *mdx* stress-related pathology. We identified downregulation of the kynurenic acid shunt, a neuroprotective branch of the kynurenine pathway, in *mdx* skeletal muscle associated with attenuated peroxisome proliferator-activated receptor-gamma coactivator 1 alpha (PGC-1α) transcriptional regulatory activity. Restoring the kynurenic acid shunt by skeletal muscle-specific PGC-1α overexpression in *mdx* mice did not prevent scruff -induced inactivity, nor did abrogating extrahepatic kynurenine pathway activity by genetic deletion of the pathway rate-limiting enzyme, indoleamine oxygenase 1. We further show that reduced $NAD^+$ production in *mdx* skeletal muscle after subordination stress exposure corresponded with elevated levels of $NAD^+$ catabolites produced by ectoenzyme cluster of differentiation 38 (CD38) that have been implicated in lethal *mdx* response to pharmacological β-adrenergic receptor agonism. However, genetic CD38 ablation did not prevent *mdx* scruff-induced inactivity. Our data do not support a direct contribution by the kynurenine pathway or CD38 metabolic dysfunction to the exaggerated stress response of *mdx* mice.

**Graphical Abstract**
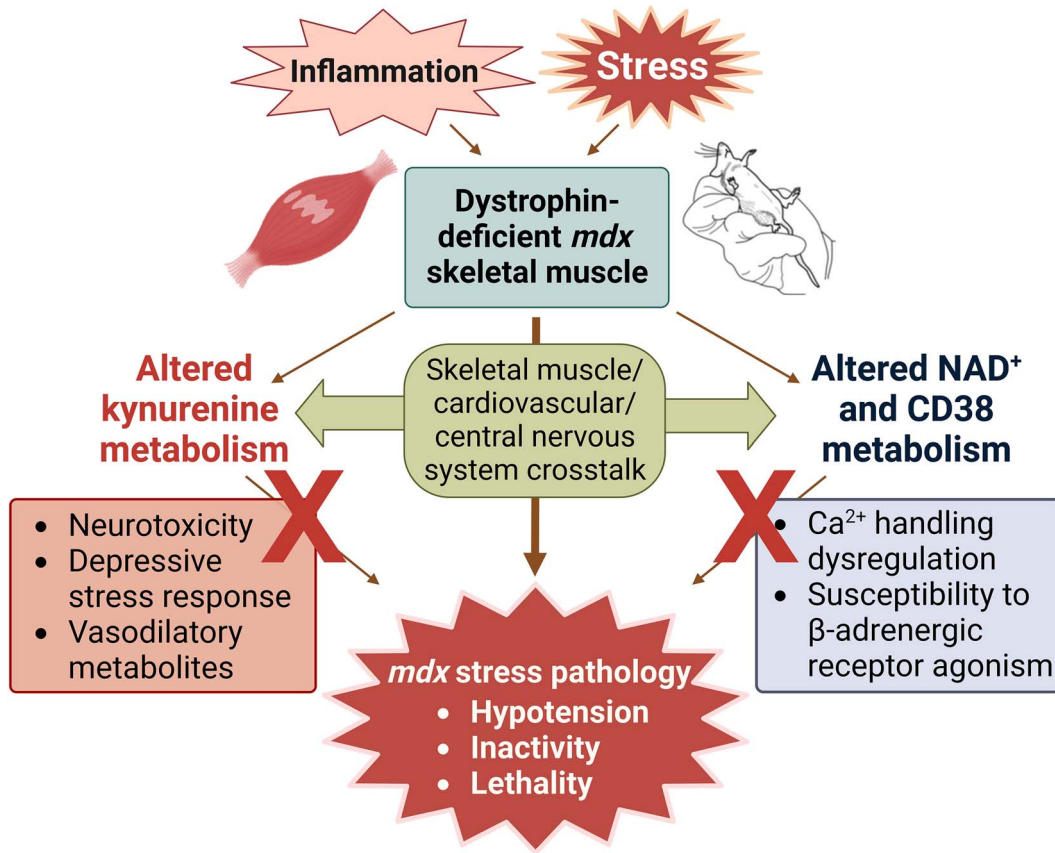
## Introduction

Duchenne muscular dystrophy (DMD) is a rare X-linked neuro-muscular disease caused by absence of the protein dystrophin. DMD currently has no cure and the median patient life expectancy is in the third to fourth decade [1]. The DMD disease course involves progressive muscle wasting and eventual failure of respiratory and cardiovascular function. Many DMD patients also suffer from underappreciated co-morbidities, including emotional, behavioral, and autonomic nervous system disorders [2, 3]. A recent study uncovered a pathological startle response exhibited by DMD patients that illustrates central nervous system (CNS) dysfunction and suggests elevated stress susceptibility in the DMD population [4]. Additionally, progressive bouts of skeletal muscle (SkM) degeneration and regeneration due to dystrophin-deficient muscle fragility lead to fibrotic deposition and a chronic inflammatory environment [5]. Cytokines produced by the peripheral immune system and within the CNS can alter brain circuitry and impact behavioral and emotional responses to stress [6, 7]. Persistent inflammation correlates with deleterious health outcomes to chronic stress in humans [8], and pathological co-regulation of social stress and immune activation has been demonstrated across species [9–12].

Recently, our lab has demonstrated that even the mildly affected *mdx* mouse model of DMD presents with lethal susceptibility to graded stress exposure [13]. Scruff handling and psychosocial stress, known as chronic subordination stress (CSS),

each provoke tonic immobility and hypotension in *mdx*, with CSS triggering up to 70% mortality within 48 h. Intriguingly, post-stress hypotension is mismatched with elevated heart rate in *mdx* mice, resulting in an increased shock index and indicating that cardiac instability may be responsible for *mdx* stress lethality. Unraveling the mechanism that drives *mdx* stress pathology is critical for research conducted using the *mdx* mouse model, given that a brief neck scruff is a routine rodent handling method and may confound behavioral and functional *mdx* studies. Stress-induced inactivity, hypotension, and lethality are rescued in the Fiona/*mdx* and MTBD/*mdx* mouse models that have full-length utrophin or dystrophin/utrophin chimeras transgenically restored exclusively in SkM, suggesting a vital role for SkM dystrophinopathy in *mdx* stress pathology. Previous work utilizing an antisense oligonucleotide exon-skipping approach to restore dystrophin systemically or with brain-specific targeting demonstrate varying degrees of protection against *mdx* scruff-induced inactivity [14–16]. Our observation that *mdx* stress-induced freezing behavior and lethality is rescued in mouse models that do not restore full-length dystrophin expression to the brain [13] suggests the existence of a SkM-CNS stress response signaling axis that is disrupted by dystrophinopathy or secondary consequences (chronic inflammation and dysregulated metabolic and cellular signaling) that modulate muscle secretion of molecules with paracrine or endocrine functions that govern inter-organ crosstalk between SkM, the cardiovascular system, and the CNS in a stress context.

The kynurenine (KYN) pathway of tryptophan degradation is one candidate metabolic pathway that could explain the hypotensive vascular component as well as the SkM specificity of the *mdx* stress response. KYN metabolism is constitutively active in the liver to catabolize tryptophan and synthesize *de novo* nicotinamide adenine dinucleotide (NAD$^+$). Extrahepatic KYN activity is catalyzed by the rate-limiting enzymes indoleamine oxygenase (IDO) 1 and 2 expressed primarily in dendritic cells [17] and is generally a pathological phenomenon triggered by persistent inflammation as a compensatory immunosuppressive response [18]. KYN pathway activation during sepsis is linked to hypotension [19], and an oxidized precursor to KYN synthesized by IDO1 has been shown to cause vasodilation in the presence of an inflammatory environment producing high levels of reactive oxygen species [18, 20]. KYN and several of its downstream metabolites can cross the blood–brain barrier and are excitotoxic acetylcholine receptor agonists [18, 21]. Elevated circulating KYN levels are observed in chronic stress exposure [22–24] and mood disorders [25–27]. Vasodilatory and neurotoxic signaling by the KYN pathway is therefore a plausible effector of the vascular and behavioral facets of *mdx* stress pathology.

The KYN pathway also regulates SkM crosstalk with the brain, vasculature, and other peripheral organs to drive exercise and physiological stress adaptations [22, 28, 29]. KYN is catabolized by KYN aminotransferase (KAT) enzymes to a neuroprotective end product, kynurenic acid (KYNA), which is unable to cross the blood-brain barrier and acts as an acetylcholine receptor antagonist [30]. This neuroprotective branch of the KYN pathway is referred to as the KYNA shunt and is regulated by the key transcriptional coactivator peroxisome proliferator-activated receptor-$\gamma$ coactivator 1$\alpha$ (PGC-1$\alpha$). SkM KYNA shunt activation shifts the KYN pathway balance toward KYNA production, disposing of neurotoxic metabolites and promoting SkM health [31–33]. MCK-PGC mice that overexpress PGC-1$\alpha$ in SkM are resilient to chronic stress-induced depression and exhibit reduced immobility time in a forced swim test, suggesting that enhanced KYNA shunt activity may prevent *mdx* stress-induced inactivity [22]. Recent evidence reveals KYN pathway alterations and reduced levels of KATs, PGC-1$\alpha$, and KYNA in the DBA/2J (D2) *mdx* mouse model of DMD [34]. Thus, the KYN pathway is a potential regulator of physiological stress responses in SkM dystrophinopathy based on its role in stress-dependent behavioral and CNS pathology as well as hypotension.

Here, we investigated whether extrahepatic KYN pathway activation contributes to *mdx* stress pathology by characterizing the KYN pathway and downstream NAD$^+$ synthetic and catabolic pathways in SkM and circulation at baseline and after graded stress exposure. We demonstrated attenuated KYNA shunt activity and reduced PGC-1$\alpha$ levels in *mdx* mice that are restored in MTBD/*mdx* mice with transgenic SkM dystrophin expression. However, we showed that neither global IDO1 ablation nor rescue of KYNA shunt function via SkM-specific PGC-1$\alpha$ expression in *mdx* mice is protective against scruff-induced inactivity, which was unexpected given the established role of the KYN pathway in cardiovascular and SkM stress physiology. We present evidence of altered NAD$^+$ metabolism and catabolic enzyme cluster of differentiation 38 (CD38) activity in *mdx* mice after SD exposure, but contrary to explanations, global CD38 ablation does not rescue *mdx* scruff-induced inactivity. Our findings provide valuable insights into *mdx* metabolic defects and argue against KYN and CD38 metabolic dysfunction as direct contributors to *mdx* stress pathology.

## Results

### KYN pathway enzyme expression is altered in *mdx* mice at baseline and after scruff stress

To probe the contribution of KYN pathway alterations to *mdx* stress pathology, we quantified transcript and protein levels of KYN pathway enzymes (Fig. 1A) in 12-week-old wild-type (WT) and *mdx* quadriceps (quad) SkM at baseline and after exposure to brief scruff stress. We confirmed that open field cage locomotion activity is dramatically reduced in *mdx* mice following scruff stress, despite similar activity levels between genotypes at baseline (Fig. 1B). The three SkM-expressed KAT transcripts—*Kyat1*, *Kyat3*, and *Got2*, which correspond to enzymes KAT1, KAT3, and KAT4, respectively—were significantly reduced in *mdx* quad muscle compared to WT (Fig. 1C). Protein levels of KAT3 and KAT4, but not KAT1, were also significantly reduced in *mdx* quad muscle independent of scruff stress (Fig. 1D–F). Consistent with previous work [34, 35], *mdx* quad also demonstrated reduced *Ppargc1a* transcript (Fig. 1C; interaction: $P = 0.04$). Interestingly, scruff stress enhanced *Ppargc1a* transcript abundance in WT but not *mdx* SkM (Fig. 1C), corresponding with an elevation in *Kyat3* and *Got2* transcript levels in WT SkM after scruff exposure that is blunted in *mdx* mice.

Lethal CSS promotes SkM inflammation in *mdx* mice that is prevented by transgenic dystrophin (MTBD/*mdx*) or utrophin (Fiona/*mdx*) overexpression in SkM, which both protect against CSS-induced mortality [13]. To test whether the more mild scruff stress imposes an analogous pro-inflammatory burden on *mdx* SkM, we quantified transcript levels for the inflammatory cytokines tumor necrosis factor (*TNF*/TNF), interleukin 6 (*Il6*/IL-6), and interleukin 1 beta (*Il1b*/IL-1$\beta$) in WT and *mdx* SkM at baseline and after scruff stress. Although cytokine transcript abundance exhibited high variability between individual *mdx* mice, all three cytokines were significantly upregulated in *mdx* SkM compared to WT muscle (Fig. 1G–I), with a trend toward higher expression in a post-scruff compared to baseline state.

Transcript abundance of rate-limiting enzyme *Ido1* was significantly elevated in WT and *mdx* quad muscle after scruff stress exposure, suggesting stress-induced extrahepatic KYN pathway activation (Fig. 1J). However, IDO1 protein was not detected in WT or *mdx* SkM by western blot analysis, using recombinant IDO1 protein and high IDO1-expressing rabbit epididymis as positive controls (Fig. S1). Downstream KYN pathway enzymes kynureninase (*Kynu*/KYNU) and 3-hydroxyanthranilate 3,4-dioxygenase (*Haao*/3-HAO) demonstrated significantly elevated transcript abundance in *mdx* SkM, and *Kynu* was further upregulated after scruff exposure in *mdx* mice (Fig. 1J; interaction: $P = 0.048$). Quinolinate phosphoribosyltransferase (*Qprt*/QPRT) catalyzes the catabolism of neurotoxic quinolinic acid (QA) to nicotinic acid mononucleotide (NAMN), a precursor for *de novo* NAD$^+$ synthesis (Fig. 1A). Transcript abundance of *Qprt* was uniquely reduced in *mdx* SkM after scruff stress (Fig. 1J; interaction: $P = 0.009$), indicating potential deficits in *mdx* SkM NAD$^+$ metabolism that may be related to KYN pathway dysfunction and stress exposure. Kynurenine monooxygenase (*Kmo*/KMO), the second rate-limiting enzyme of the KYN pathway, exhibited significant transcript-level upregulation in scruff-exposed *mdx* quad muscle, while KMO protein abundance was significantly elevated in *mdx* quad compared to WT muscle at baseline and decreased between baseline and scruff-exposed *mdx* SkM (Fig. 1J; interaction: $P = 0.002$; Fig. 1K; interaction: $P = 0.044$). These data suggest KYN pathway dysregulation in *mdx* SkM and divergent transcript-and protein-level pathway regulation.
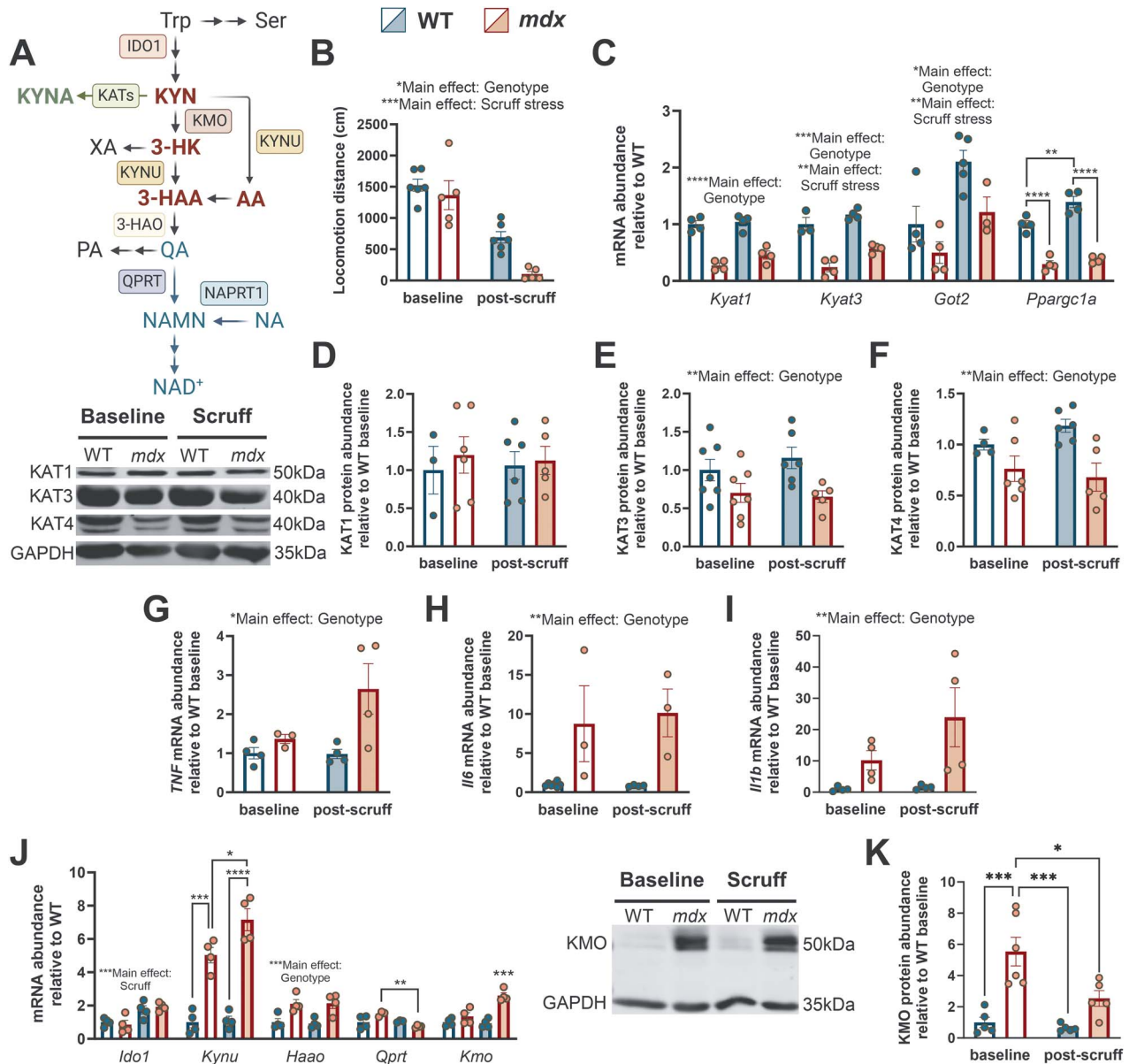
**Figure 1.** Kynurenine pathway enzyme abundance is altered in *mdx* skeletal muscle and corresponds with reduced PGC-1α and elevated cytokine abundance. (A) Schematic KYN metabolic pathway overview, with neurotoxic branch enzymes (IDO1, KMO) in red, the KYNA shunt (KYNA, KAT enzymes) in green, and *de novo* NAD⁺ synthesis metabolites (QA, NAMN, NA, NAD⁺) in blue (created with BioRender.com). (B) Open field activity cage horizontal locomotion activity in WT and *mdx* mice as a readout for scruff stress response in WT and *mdx* mice, with distances presented as a 30 min total before and after a 30 s scruff exposure. (C–F) qPCR and western blot analysis of KAT enzyme and *Ppargc1a* abundance in quad muscles from WT and *mdx* mice at baseline and after scruff stress. (G–I) qPCR analysis of mRNA levels of cytokines in quad muscles from WT and *mdx* mice at baseline and after scruff stress. (J and K) qPCR and western blot analysis of neurotoxic KYN pathway enzyme abundance in quad muscles from WT and *mdx* mice at baseline and after scruff stress. Bar graphs depict mean values (±SEM) from n = 4–7 mice/group. Comparisons between groups were made using two-way ANOVA with Tukey's multiple comparisons test (*$P < 0.05$; **$P < 0.01$; ***$P < 0.001$; ***$P < 0.0001$).

## Altered stress-related neurotoxic KYN pathway metabolites in *mdx* plasma

To assess KYN pathway dynamics under basal and stress-exposed conditions, we quantified KYN metabolites in plasma from healthy and *mdx* mice at baseline and 30 min after scruff stress. As a comparison between mild and severe physiological stressors, we also analyzed KYN metabolites from mice exposed to an acute version of CSS termed social defeat (SD) stress, in which tissues were collected at the 6-h time point following CSS onset. We have previously demonstrated that plasma corticosterone is elevated in *mdx* mice at the 30 min post-scruff and 6 h mid-CSS intervals [13], suggesting that relevant stress-induced metabolic alterations may be captured at these time points. The MTBD/*mdx* mouse, which expresses a full-length dystrophin/utrophin chimera in SkM and is protected against scruff-induced inactivity and SD-induced lethality [13], was included to assess whether MTBD/*mdx* stress resilience corresponds with improved KYN pathway function. A customized targeted multiple reaction monitoring (MRM) liquid chromatography–tandem mass spectrometry (LC-MS/MS)-based KYN metabolite panel was adapted from previous work [36, 37] and performed using plasma collected from separate cohorts of WT, *mdx*, and MTBD/*mdx* mice at baseline, 30 min after scruff stress, or 6 h after SD stress. Despite elevated *Ido1* transcript abundance in SkM after scruff exposure (Fig. 1G),
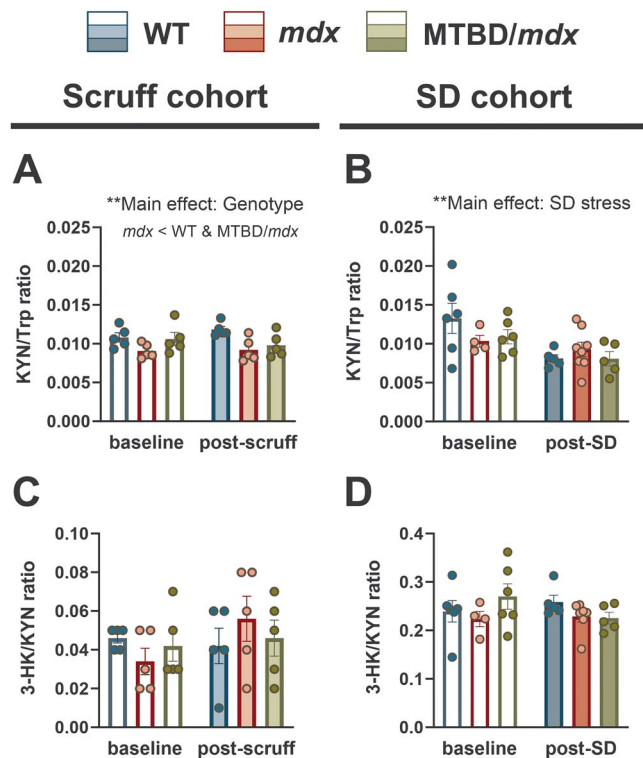
**Figure 2.** Circulating neurotoxic KYN pathway metabolites ratios indicate reduced peripheral IDO1 activity in *mdx* mice. (A and B) Targeted metabolomics analysis of plasma KYN and Trp metabolite levels presented as a ratio to represent peripheral IDO1 enzymatic activity in WT, *mdx*, and MTBD/*mdx* mice at baseline, after scruff stress (A), or after social defeat stress (B). (C and D) Plasma 3-HK and KYN metabolite levels presented as a ratio to represent peripheral KMO enzymatic activity in WT, *mdx*, and MTBD/*mdx* mice at baseline, after scruff stress (C), or after social defeat stress (D). Bar graphs depict mean values (±SEM) from n = 4–8 mice/group. Comparisons between groups were made using two-way ANOVA with Tukey's multiple comparisons test (*$P < 0.05$; **$P < 0.01$; ***$P < 0.001$; ***$P < 0.0001$).

neither scruff nor SD stress corresponded to an elevation in the ratio of KYN to tryptophan (Trp), which serves as proxy for peripheral IDO1 activity (Fig. 2A and B). Instead, a minor but significant decrement in the KYN/Trp ratio was observed in the *mdx* scruff cohort (Fig. 2A), while SD was associated with an overall significant reduction in IDO1 activity across genotypes (Fig. 2B). The ratio of 3-hydroxykynurenine (3-HK) to KYN, a proxy for peripheral KMO activity, was unchanged across genotypes and stress conditions (Fig. 2C and D). Absolute Trp and 3-HK levels exhibited a scruff-dependent elevation across genotypes, with a significant reduction in MTBD/*mdx* circulating Trp content in the SD cohort (Fig. 3A–D).

Based on transcript data indicating elevated KYNU and 3-HAO enzyme abundance in *mdx* SkM, we compared the ratios of 3-hydroxyanthranilic acid (3-HAA) to 3-HK or QA to 3-HAA as proxies for peripheral KYNU and 3-HAO activity, respectively. The 3-HAA/3-HK ratio was unchanged across genotypes while the QA/3-HAA ratio was significantly reduced in *mdx* plasma independent of scruff exposure (Fig. 3E and F). Quantifications for 3-HAA were not made for the SD cohort due to poor chromatographic resolution; therefore, KYNU and 3-HAO enzymatic activity could not be assessed. Absolute circulating QA levels (Fig. 3G and H), as well as its catabolic product, picolinic acid (PA; Fig. 3I and J), were reduced in both scruff and SD *mdx* cohorts compared to WT, with a deficit compared to MTBD/*mdx* mice also evident in the scruff

cohort (Fig. 3G and I). The reduced QA/3-HAA ratio in *mdx* plasma does not reflect elevated *Haao* transcript levels in *mdx* SkM, which may be explained by low expression of 3-HAO in SkM. The low correspondence of intermediate KYN pathway enzyme expression in SkM with circulating metabolite levels suggests an overall minor contribution of SkM to the neurotoxic KYN pathway outside of KYNA shunt regulation. However, the observed depletion of QA in *mdx* circulation suggests reduced intermediate *mdx* KYN pathway flux and substrate availability for *de novo* NAD$^+$ synthesis that may be influenced by dystrophinopathy beyond the SkM. Overall, *mdx* and MTBD/*mdx* mice exhibited similar neurotoxic KYN metabolite levels in plasma at the post-stress time points assessed, suggesting that differences in stress responses between dystrophin-deficient and dystrophin-replete mice may be driven by transient changes in circulating neurotoxic KYN metabolites at an earlier time point than we measured or by an alternative mechanism beyond the KYN pathway.

## Ablation of IDO1 fails to rescue scruff-induced inactivity in *mdx* mice

To directly test the role of the extrahepatic KYN pathway in mediating the exaggerated stress responses of *mdx* mice, we pharmacologically inhibited and genetically ablated the pathway's rate limiting enzyme, IDO1. Pretreatment with the IDO1 inhibitor 1-MT did not prevent *mdx* scruff-induced inactivity (Fig. 4A). To avoid the potentially stressful handling of mice associated with administration of 1-MT, we crossed mice with global IDO1 deletion onto an *mdx* background (IDO-KO/*mdx*) to characterize stress resiliency in a genetic *mdx* model lacking extrahepatic KYN pathway activity through the primary rate-limiting enzyme. We verified IDO1 genetic ablation in quad muscle, lungs, and spleen with qRT-PCR (Fig. 4B). IDO1 mediates immunosuppressive signaling [38, 39], and we confirmed that loss of IDO1 immunoregulation corresponded with elevated transcript levels of cytokines IL-6, and IL-1$\beta$, but not TNF, in IDO-KO/*mdx* quad muscle compared with *mdx* mice (Fig. 4C–E). Neither heterozygous (IDO$^{+/-}$/*mdx*) nor homozygous (IDO-KO/*mdx*) knockout mice were protected against scruff-induced inactivity (Fig. 4F), indicating that IDO1-catalyzed KYN pathway activity does not mediate the aberrant behavioral response to scruff in *mdx* mice.

## Transgenic SkM dystrophin expression rescues the KYNA shunt in *mdx* mice

We demonstrated that murine SkM does not express appreciable levels of IDO1 protein (Fig. S1) and whole-body IDO1 ablation does not prevent *mdx* scruff-induced inactivity (Fig. 4F). The SkM KYNA shunt is an established regulator of the peripheral KYN pathway independent of IDO1 and disposes of excess circulating neurotoxic KYN by producing KYNA, a neuroprotective metabolite associated with increased stress resiliency [22]. Based on observed deficits in *Ppargc1a* and KAT enzyme abundance in dystrophin-deficient SkM (Fig. 1C, E and F), we hypothesized that reduced KYNA shunt activity drives *mdx* stress pathology. Therefore, we assessed whether stress-resilient MTBD/*mdx* mice expressing SkM dystrophin present with a restored KYNA shunt and improved balance between KYN and KYNA production. While basal circulating KYNA levels were similar between *mdx* and MTBD/*mdx* mice (Fig. 5A), genotype had a significant effect on plasma KYN levels in the SD cohort, with a trend toward reduced KYN in MTBD/*mdx* plasma (Fig. 5E). Additionally, scruff-dependent elevation in circulating KYNA and KYN was significantly blunted in *mdx* mice (Fig. 5A and B), while SD stress depleted plasma KYNA levels and did not affect KYN content across genotypes (Fig. 5D and E). The
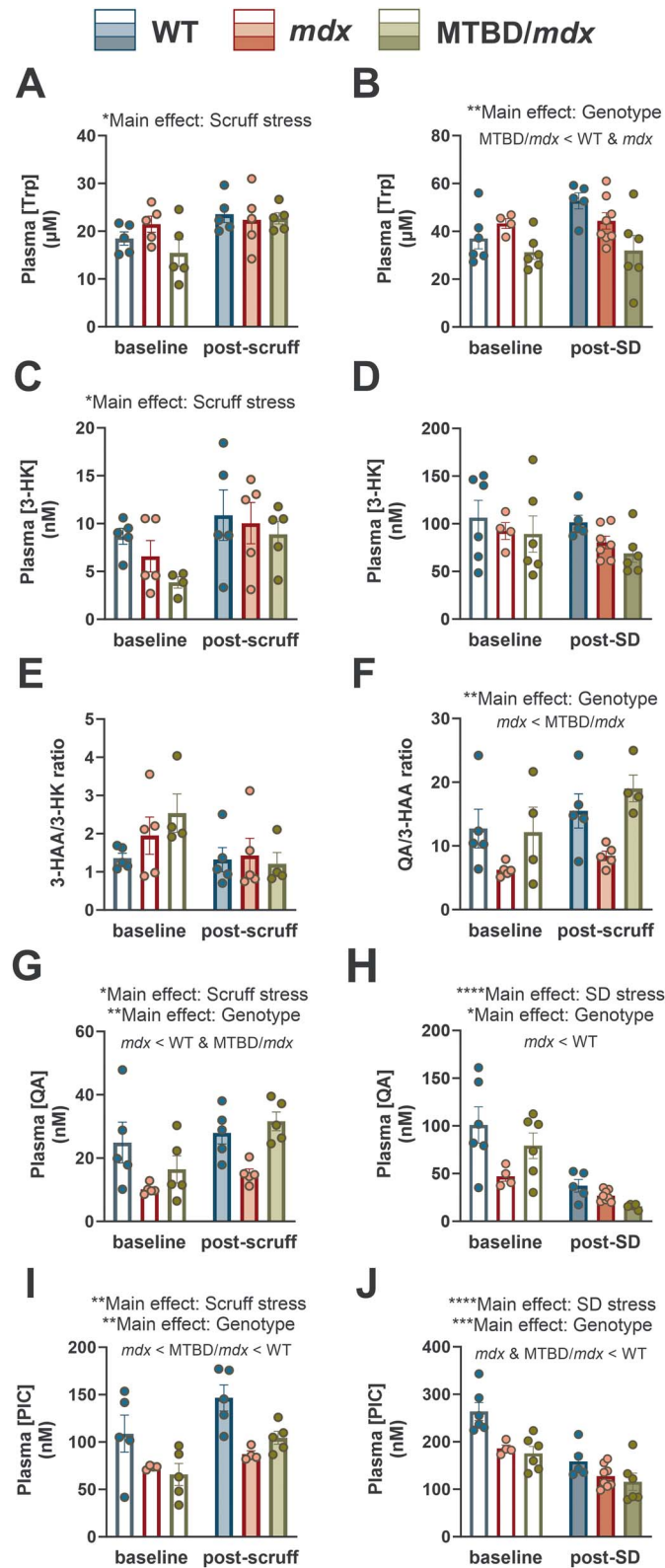
**Figure 3.** Circulating KYN pathway intermediate metabolite levels are variably altered by skeletal muscle dystrophinopathy and stress exposure, while NAD+ precursor quinolinic acid is reduced in mdx plasma and in all genotypes after social defeat stress. (A and B) Plasma tryptophan metabolite levels in WT, mdx, and MTBD/mdx mice at baseline, after scruff stress (A), or after social defeat stress (B). (C and D) Plasma 3-hydroxykynurenine (3-HK) metabolite levels in WT, mdx, and MTBD/mdx mice at baseline, after scruff stress (C), or after social defeat stress (D). (E) Plasma 3-hydroxyanthranilic acid (3-HAA) and 3-HK metabolite levels expressed as a ratio to represent kynureninase enzymatic activity in WT, mdx, and MTBD/mdx mice at baseline or after scruff stress. (F) Plasma quinolinic acid (QA) and 3-HAA metabolite levels expressed as a ratio to represent quinolinate phosphoribosyl transferase enzymatic activity in WT, mdx, and MTBD/mdx mice at baseline or after scruff stress. (G and H) Plasma QA metabolite levels in WT, mdx, and MTBD/mdx mice at baseline, after scruff stress (G), or after social defeat stress (H). (I and J) Plasma picolinic acid metabolite levels in WT, mdx, and MTBD/mdx mice at baseline, after scruff stress (I), or after social defeat stress (J). Bar graphs depict mean values ($\pm$SEM) from $n = 4$–8 mice/group. Comparisons between groups were made using two-way ANOVA with Tukey's multiple comparisons test (*$P < 0.05$; **$P < 0.01$; ***$P < 0.001$; ***$P < 0.0001$).
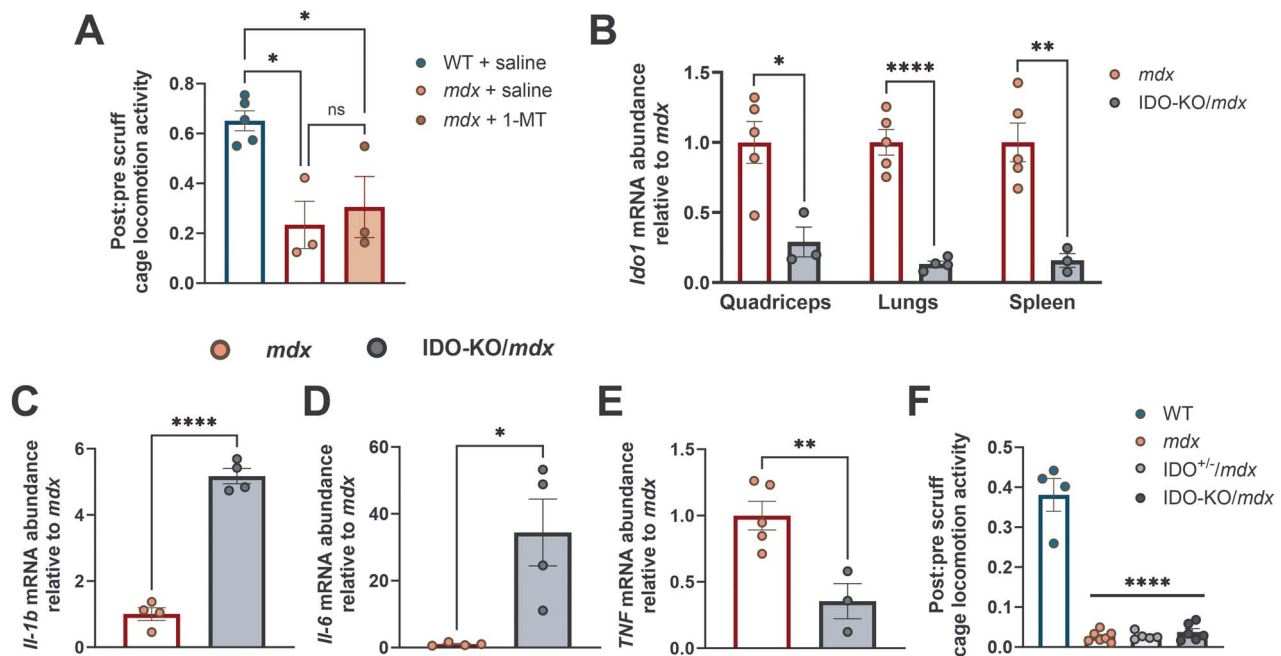
**Figure 4.** Global pharmacological IDO1 inhibition and genetic IDO1 ablation do not prevent scruff -induced inactivity in *mdx* mice. (A) Ratio of open field horizontal locomotion distance for 30 min before and after a 30 s scruff exposure in WT and *mdx* mice treated intraperitoneally (i.p.) with saline, as well as *mdx* mice treated i.p. with 80 mg/kg 1-methyltryptophan (1-MT). (B) qPCR analysis of mRNA levels of IDO1 in quad, lung, and spleen tissue from *mdx* and IDO-KO/*mdx* mice with both alleles deleted for IDO1. (C–E) qPCR analysis of cytokine mRNA abundance in quad muscle from *mdx* and IDO-KO/*mdx* mice. (F) Ratio of open field horizontal locomotion distance for 30 min before and after a 30 s scruff exposure in WT, *mdx*, and heterozygous (IDO$^{+/-}$/*mdx*) and homozygous IDO-KO/*mdx* mice. Bar graphs depict mean values (±SEM) from n = 3–8 mice/group. Comparisons between groups were made using two-tailed unpaired t test or one-way ANOVA with Tukey's multiple comparisons test (*$P < 0.05$; **$P < 0.01$; ***$P < 0.001$; ***$P < 0.0001$).

plasma KYNA/KYN ratio, which is used to represent peripheral KAT enzymatic activity, was significantly reduced in *mdx* mice independent of stress exposure and was not different from the WT ratio in MTBD/*mdx* plasma (Fig. 5C and F). A significant main effect was observed for both scruff and SD stress in modifying the KYNA/KYN ratio (Fig. 5C and F), reflecting elevation and depletion of KYNA levels after scruff and SD stress exposure, respectively. Overall, these data demonstrate a significant reduction in circulating neurotoxic KYN levels and significantly increased KAT activity in MTBD/*mdx* mice, suggesting that SkM dystrophin expression restores the *mdx* peripheral KYNA shunt.

## PGC-1α overexpression rescues the KYNA shunt but not scruff-induced inactivity in *mdx* mice

Given that MTBD/*mdx* mice have normal KYNA shunt function (Fig. 5C and F) and also present with WT-like post-scruff activity [13], we hypothesized that overexpression of PGC-1α, a regulator of the SkM KYNA shunt [22, 31], would likewise lead to protection from scruff in *mdx* mice. We therefore generated transgenic *mdx* mice that overexpress PGC-1α exclusively in SkM [40]. PGC-1α and KAT transcript content was restored to WT levels in MTBD/*mdx* SkM, while SkM-specific PGC-1α overexpression in *mdx* mice (PGC-*mdx*) was validated to significantly enhance *Ppargc1a*, *Kyat3*, and *Got2* transcript levels over all other genotypes (Fig. 6A). Notably, protein-level KAT expression in PGC-*mdx* SkM displayed isoform dependence, with a significant elevation in KAT1 and KAT4, but not KAT3, protein levels in PGC-*mdx* quad muscle (Fig. 6B–D). Despite upregulation of KAT expression in PGC-*mdx* SkM, PGC-*mdx* mice were not protected from scruff-induced inactivity (Fig. 6E).

Previous work has demonstrated that SkM PGC-1α overexpression leads to increased utrophin expression in *mdx* mice [35, 41]. We have shown that transgenic SkM utrophin

overexpression in the Fiona/*mdx* mouse prevents scruff-induced inactivity [13], (Fig. 6E). Since PGC/*mdx* mice displayed *mdx*-like scruff-induced inactivity (Fig. 6E), we compared utrophin protein levels between WT, *mdx*, PGC/*mdx*, and Fiona/*mdx* mice to determine whether the magnitude of utrophin overexpression influences *mdx* scruff susceptibility. WT, *mdx*, and PGC/*mdx* utrophin protein levels in quad, gastrocnemius (GAS), soleus (SOL), and extensor digitorum longus (EDL) muscle were similar, while Fiona/*mdx* mice exhibited significant utrophin upregulation compared to WT (quad: 77-fold; GAS: 12-fold; SOL: 3-fold; EDL: 17-fold) (Fig. 6F). These results suggest that any mild utrophin upregulation observed in PGC/*mdx* SkM is not sufficient to prevent scruff-induced inactivity. Altogether, these data demonstrate a persistence of aberrant *mdx* scruff responsiveness despite restoration of the SkM KYNA shunt and PGC-1α transcriptional regulation. SkM-regulated KYN buffering via the KYNA shunt and overall KYN pathway dysfunction do not appear to play a central role in *mdx* behavioral scruff pathology.

## Basal and stress-induced CD38 and NAD$^+$ metabolic dysfunction in *mdx* mice

Dystrophin-deficient *mdx* mouse and DMD patient SkM both present with an NAD$^+$ deficit [42–44], but there is conflicting evidence regarding the efficacy of therapeutic attempts to replete NAD$^+$ via nicotinamide riboside (NR) and the salvage pathway (Fig. 7A) in *mdx* mice [42, 45, 46]. Because the *de novo* NAD$^+$ precursor QA is reduced in *mdx* plasma (Fig. 3G and H), we assessed whether KYN pathway flux contributes to *mdx* NAD$^+$ deficits. We performed targeted MRM LC-MS/MS metabolomics to characterize NAD$^+$ synthesis and catabolism in quad muscle (Fig. 7) and plasma (Fig. 8) from WT, *mdx*, and MTBD/*mdx* mice
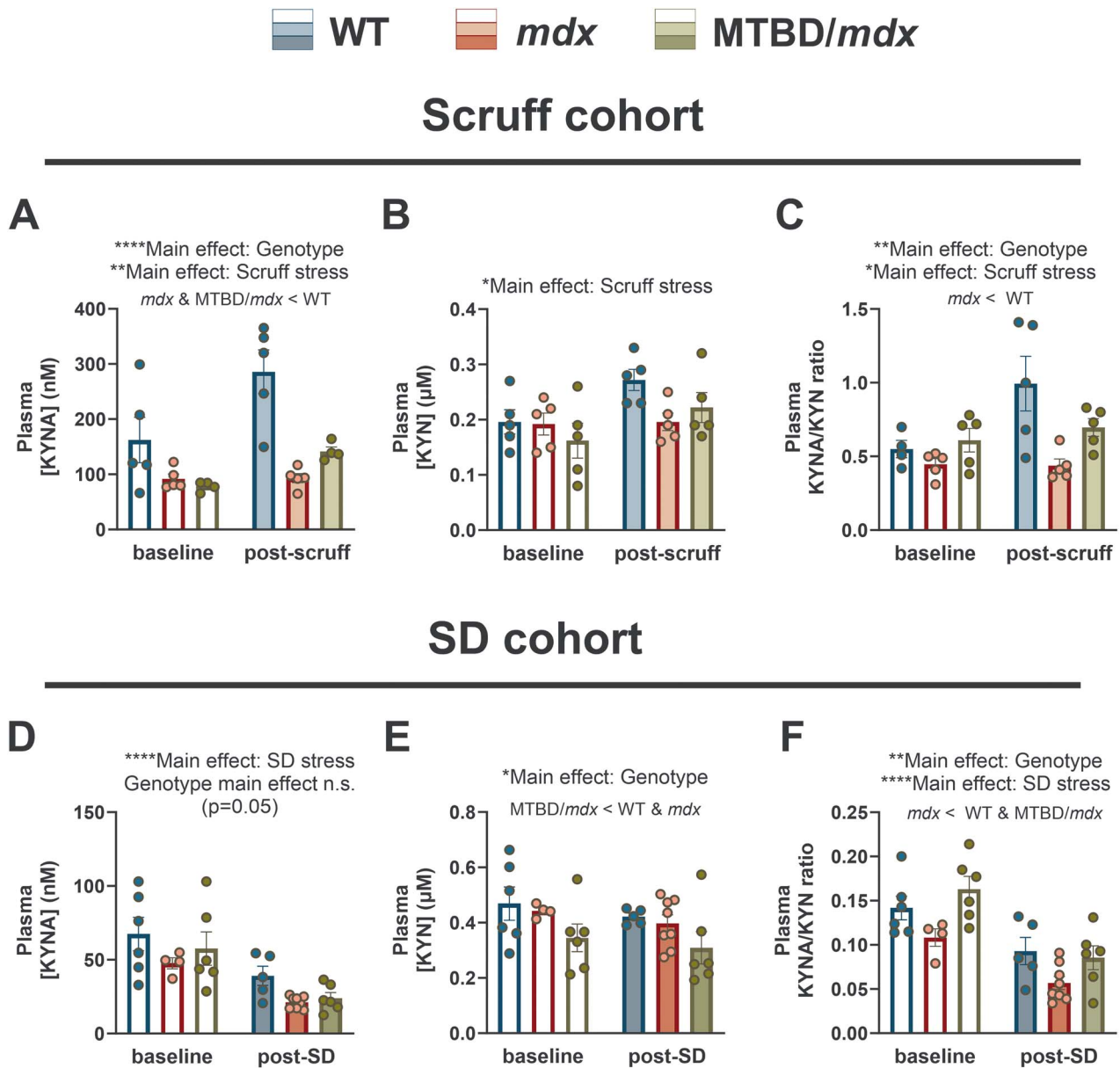
**Figure 5.** Circulating KYNA and KYN levels indicate that KYNA shunt activity is reduced in *mdx* mice and restored in MTBD/*mdx* mice. (A and C) Targeted metabolomics analysis of plasma KYNA and KYN metabolite levels in WT, *mdx*, and MTBD/*mdx* mice at baseline, after scruff stress (A), or after social defeat stress (C). (B and D) Plasma KYNA and KYN metabolite levels presented as a ratio to represent KAT enzymatic activity in WT, *mdx*, and MTBD/*mdx* mice at baseline, after scruff stress (B), or after social defeat stress (D). Bar graphs depict mean values (±SEM) from n = 4–8 mice/group. Comparisons between groups were made using two-way ANOVA with Tukey's multiple comparisons test (*$P < 0.05$; **$P < 0.01$; ***$P < 0.001$; ***$P < 0.0001$).

at baseline and after SD stress, a condition that more starkly depletes QA across genotypes than scruff stress (Fig. 3H). Our results indicate a reduction in NAD$^+$ content in *mdx* SkM, with a non-significant trend between WT and baseline *mdx* ($P = 0.058$) muscle and a significant reduction in post-SD *mdx* SkM compared to WT and MTBD/*mdx* muscle (Fig. 7B; interaction: $P = 0.016$), as well as a non-significant trend ($P = 0.079$) toward elevated absolute NADH content in *mdx* SkM (Fig. 7C; interaction: $P = 0.004$). Dystrophin-deficient *mdx* SkM exhibits a shift toward a reduced NAD$^+$/NADH ratio at baseline, and all groups demonstrate a shift toward reduction after a SD stress exposure (Fig. 7D; interaction: $P = 0.004$). This data suggests that the lowered NAD$^+$/NADH ratio observed in *mdx* SkM and across all genotypes following SD stress may be reflective of depleted NAD$^+$ due to catabolism rather than reduction to NADH. Similar to SkM, plasma levels of NAD$^+$

were reduced after SD stress exposure across genotypes (Fig. 8A). However, NADH could not be accurately quantified in our plasma samples, preventing us from determining whether a shift toward NAD$^+$ catabolism or reduction to NADH explains lower circulating NAD$^+$ levels in a post-SD condition.

Preiss-Handler pathway metabolites nicotinic acid (NA), nicotinic acid mononucleotide (NAMN), and nicotinic acid adenine dinucleotide (NAAD) have been reported to be at low abundance and demonstrate suboptimal chromatographic peak shape in plasma and SkM [36, 47]. Indeed, we were unable to quantify NA, NAMN, and NAAD using our LC-MS/MS targeted metabolomics method. However, metabolic intermediates in the NAD$^+$ salvage and CD38-catalyzed catabolic pathways were quantified with the exception of nicotinamide (NAM) in SkM, which was above the instrument LOD, potentially due to sample matrix effects.
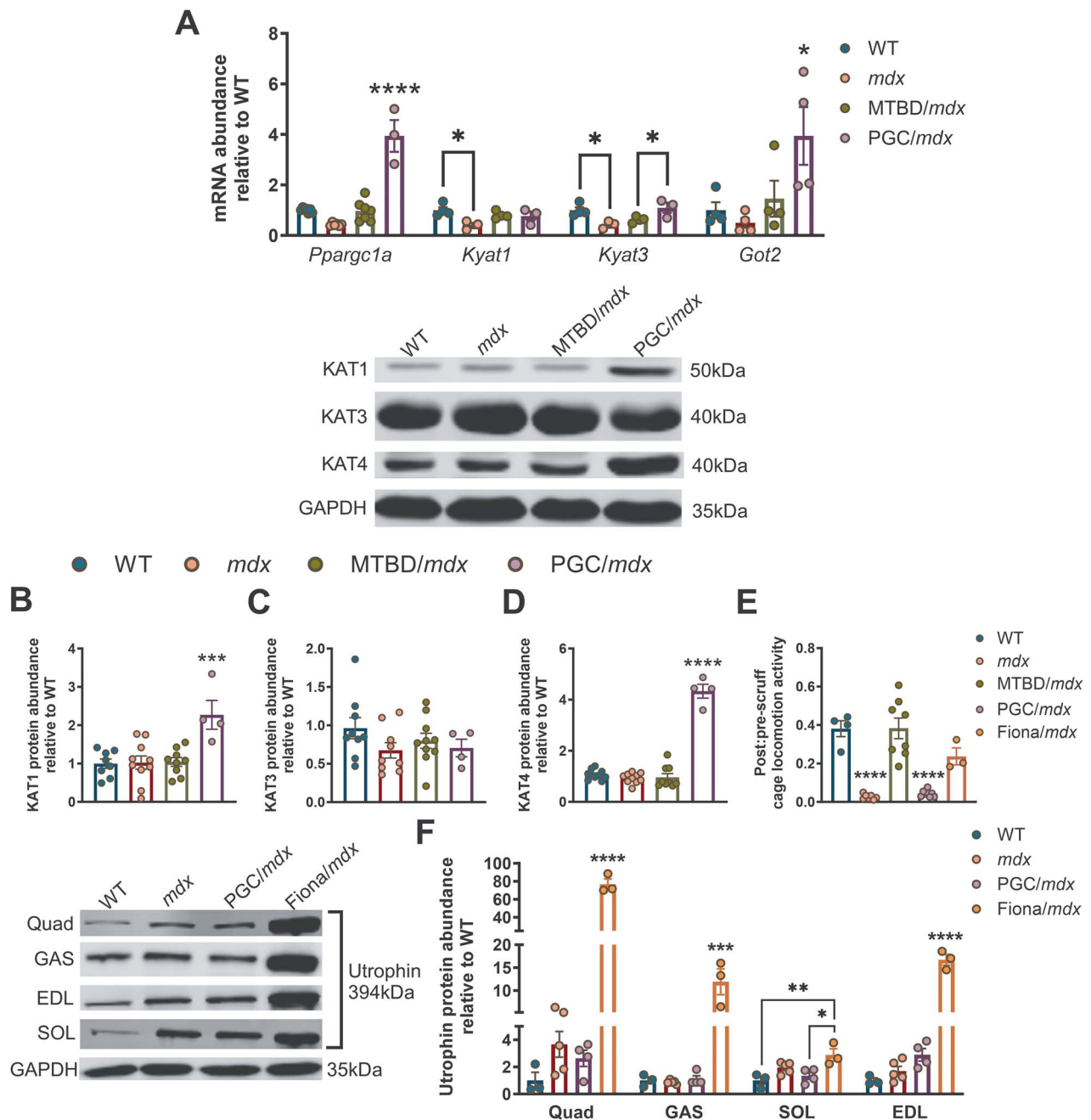
**Figure 6.** PGC-*mdx* mice exhibit elevated KAT enzyme abundance but are not protected against *mdx* scruff-induced inactivity. (A–D) qPCR and western blot analysis of *Ppargc1a* mRNA abundance and KAT enzyme abundance in quad muscle from WT, *mdx*, MTBD/*mdx*, and PGC-*mdx* mice. (E) Ratio of open field horizontal locomotion distance for 30 min before and after a 30 s scruff exposure in WT, *mdx*, MTBD/*mdx*, PGC-*mdx*, and Fiona/*mdx* mice. (F) Western blot analysis of utrophin protein abundance in WT, *mdx*, PGC/*mdx*, and Fiona/*mdx* quad, gastrocnemius (GAS), soleus (SOL), and extensor digitorum longus (EDL) muscle. Bar graphs depict mean values (±SEM) from n = 3–8 mice/group. Comparisons between groups were made using one-way ANOVA with Tukey's multiple comparisons test (*$P < 0.05$; **$P < 0.01$; ***$P < 0.001$; ***$P < 0.0001$).

Both *mdx* and MTBD/*mdx* mice exhibited elevated circulating levels of NR (Fig. 8B), a salvage pathway substrate that is metabolized to NAD$^+$ via enzymatic conversion to either NAM or nicotinamide mononucleotide (NMN). SkM NR content was not altered among groups (Fig. 7E). In accord with elevated plasma NR content, NAM levels were increased in *mdx* and MTBD/*mdx* plasma (Fig. 8C). However, NMN content was not significantly different between groups in plasma or SkM (Figs 7F and 8D). Finally, CD38 catabolic product adenosine 5'-diphosphoribose (ADPR) exhibited SD-dependent elevation that resulted in an increased ratio of ADPR to NAD$^+$ in *mdx* SkM (Fig. 7G and H). In comparison, CD38 catabolite cyclic ADPR (cADPR) was also elevated relative to NAD$^+$ after SD stress, but absolute cADPR content was reduced in *mdx* SkM (Fig. 7I; interaction: $P = 0.004$; Fig. 7J). Circulating ADPR and cADPR levels were not significantly altered between groups (Fig. 8E and G). However, the ratio of each CD38 metabolite to NAD$^+$ did exhibit SD-dependent elevations in *mdx* and MTBD/*mdx* plasma (Fig. 8F and H), corresponding to increased circulating NAM content. Altogether, these data suggest altered NAD$^+$ flux through salvage and catabolic pathways that support increased CD38 activity in dystrophin-deficient mice after exposure to a psychosocial stressor to which *mdx* mice are lethally susceptible.
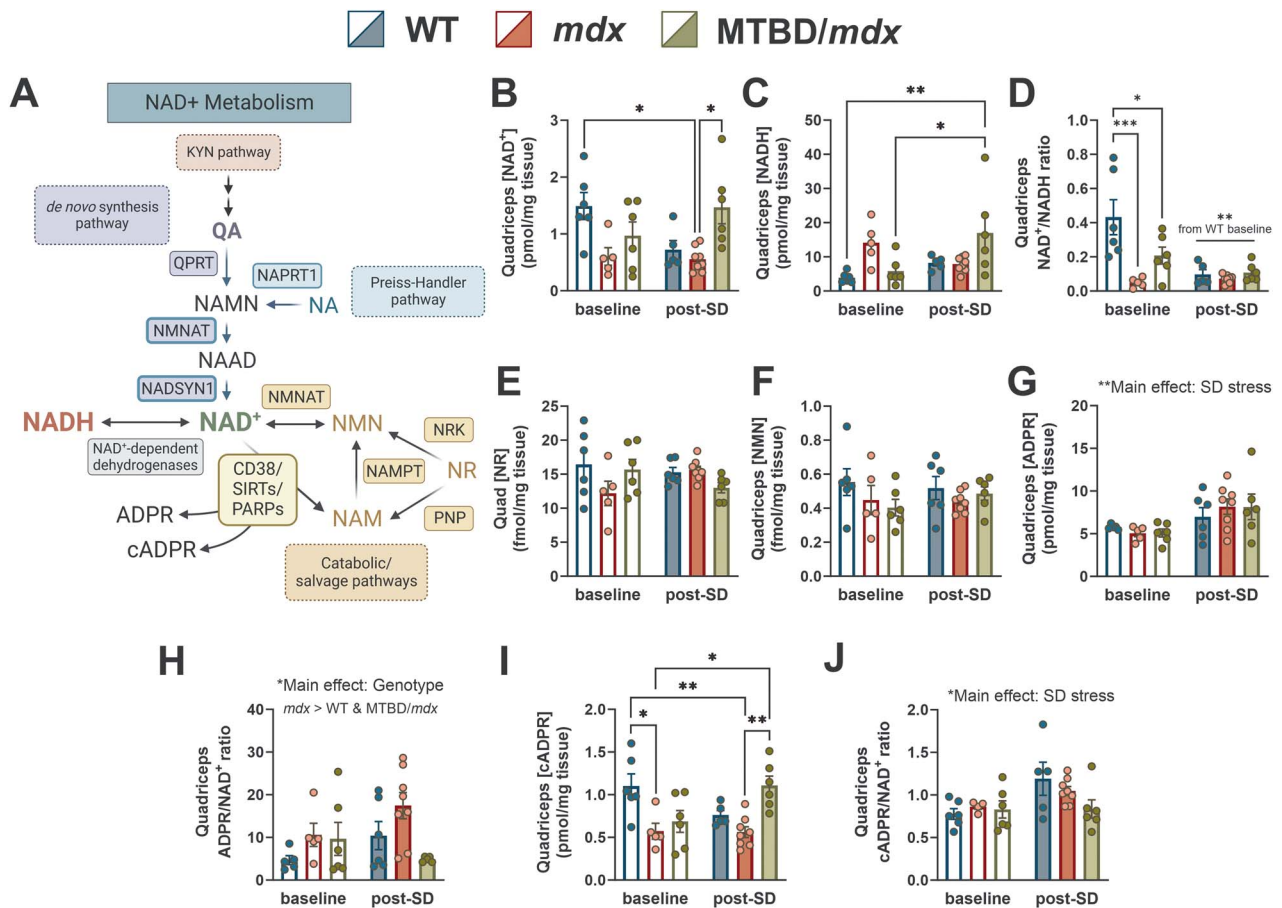
**Figure 7.** NAD$^+$ metabolic defects in *mdx* SkM are associated with elevated CD38 metabolites. (A) Schematic NAD$^+$ metabolic pathway overview, with *de novo* NAD$^+$ synthesis intermediates (QA, NAMN, NAAD) and enzymes (QPRT, NMNAT, NADSYN1) in purple, Preiss-handler pathway intermediate (NA) and enzymes (NAPRT1, NMNAT, NADSYN1) shaded or outlined in blue, and catabolic and savage pathway intermediates (NR, NMN, NAM) and enzymes (NRK, PMP, NAMPT, NMNAT, CD38, SIRTs, PARPs) in yellow (created with BioRender.com). (B–D) Targeted metabolomics analysis of (A) NAD$^+$, (B) NADH, and (C) NAD$^+$ and NADH expressed as a ratio in quad muscle from WT, *mdx*, and MTBD/*mdx* mice at baseline or after social defeat stress. (E and F) Targeted metabolomics analysis of (E) NR and (F) NMN in quad muscle from WT, *mdx*, and MTBD/*mdx* mice at baseline or after social defeat stress. (G–J) Targeted metabolomics analysis of absolute ADPR (G) and cADPR (I) levels, as well as their ratios respective to NAD$^+$ (H and J) to represent CD38 activity in quad muscle from WT, *mdx*, and MTBD/*mdx* mice at baseline or after social defeat stress. Bar graphs depict mean values (±SEM) from n = 4–8 mice/group. Comparisons between groups were made using two-way ANOVA with Tukey's multiple comparisons test (*P < 0.05; **P < 0.01; ***P < 0.001; ***P < 0.0001).

CD38 metabolic activity was recently demonstrated to drive lethal $\beta$-adrenergic agonist-induced cardiac arrhythmia in *mdx* mice, and global CD38 ablation improves cardiac and SkM pathology in young and aged *mdx* mice [43]. Our NAD$^+$ pathway metabolomics data (Figs 7 and 8) aligns with published targeted metabolomics data reporting CD38 hyperactivity in *mdx* SkM [43]. We employed a complementary fluorescence-based enzymatic assay [48] to confirm significantly elevated basal CD38 hydrolase (ADPR production) and cyclase (cADPR production) activity in *mdx* quad muscle compared to WT muscle at baseline and after scruff or SD stress (Fig. 9A and B). Next, we generated *mdx* mice with global CD38 genetic ablation (CD38-KO/*mdx*) to determine whether SkM CD38 hyperactivity drives *mdx* susceptibility to physiological stress. We verified that elevated CD38 hydrolase and cyclase activity in *mdx* quad muscle is dramatically attenuated in CD38-KO/*mdx* muscle (Fig. 9C and D). We also validated *Cd38* transcript ablation in CD38-KO/*mdx* cardiac and quad muscle with qRT-PCR (Fig. 9E). We tested scruff stress susceptibility in CD38-KO/*mdx* mice, but did not observe protection from exaggerated scruff-induced inactivity (Fig. 9F). Our data confirm CD38 hyperactivity in *mdx* SkM, but do not support a role for CD38

in *mdx* pathological responses to physiological stress exposure. Instead, these results suggest that distinct mechanisms regulate *mdx* cardiac susceptibility to $\beta$-adrenergic agonism and stress pathology resulting from scruff handling.

## Discussion

To elucidate metabolic contributions to *mdx* stress pathology, we characterized KYN metabolism in *mdx* mice under basal or stress-exposed conditions along two main branches: neurotoxic KYN metabolism and the neuroprotective KYNA shunt. Contrary to our hypothesis, *mdx* mice do not exhibit elevated circulatory levels of neurotoxic KYN metabolites that would indicate KYN pathway hyperactivation in response to physiological stress. Global genetic ablation of extrahepatic KYN pathway rate-limiting enzyme IDO1 on an *mdx* background also had no protective effect on the *mdx* scruff-induced inactivity phenotype. Our findings demonstrate a defect in the KYNA shunt in *mdx* mice, consistent with a recent report that showed reduced SkM PGC-1$\alpha$ and KAT expression, as well as lower KYNA levels, in the more severely affected D2-*mdx* mouse compared with WT mice [34]. Evidence from
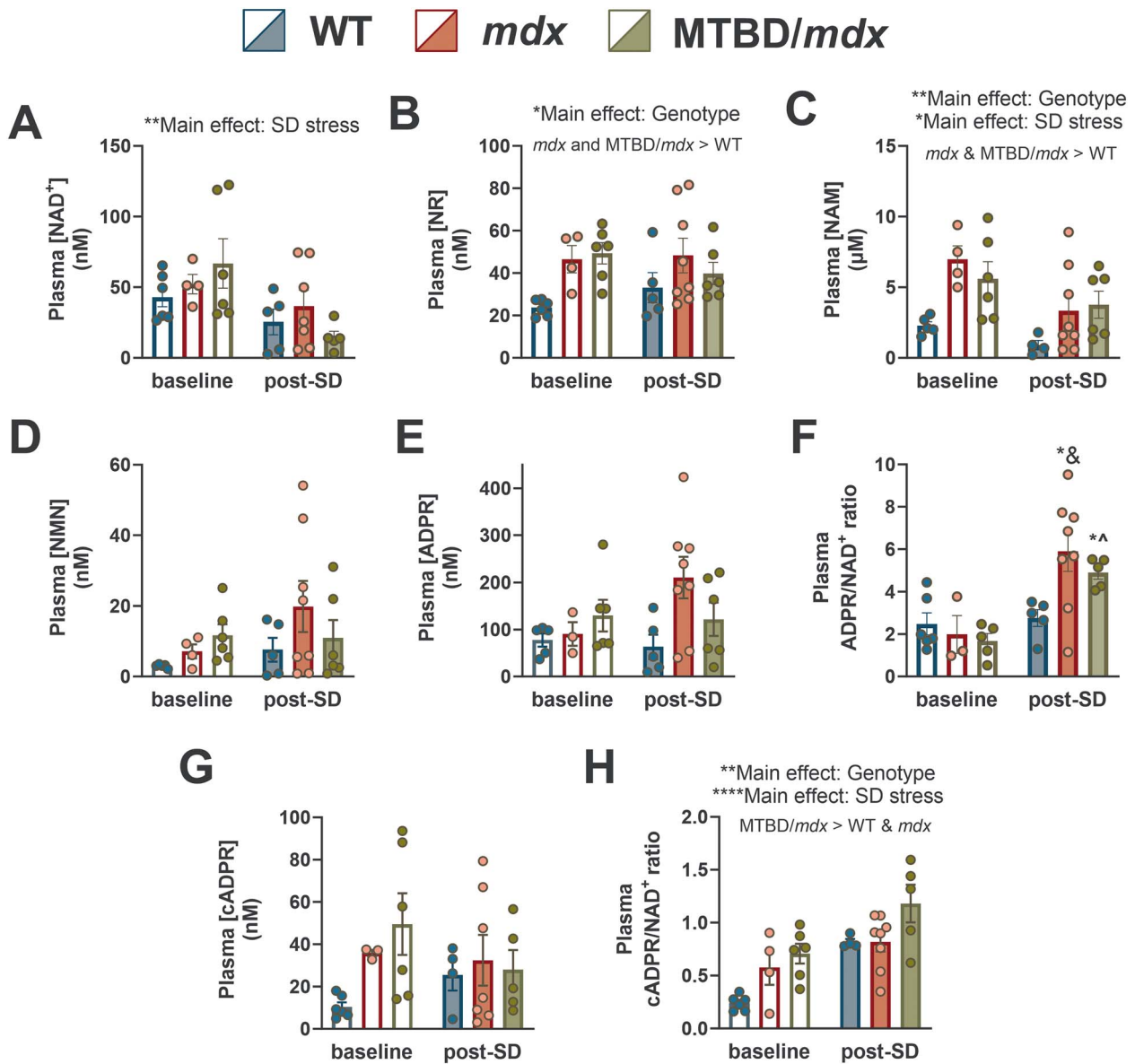
**Figure 8.** NAD$^+$ metabolic intermediates in *mdx* plasma demonstrate dystrophinopathy-and stress-dependent alterations. (A–D) Targeted metabolomics analysis of NAD$^+$ (A), NR (B), NAM (C), and NMN (D) metabolite levels in WT, *mdx*, and MTBD/*mdx* plasma at baseline or after social defeat stress. (E–H) Targeted metabolomics analysis of absolute ADPR (E) and cADPR (G) levels, as well as their ratios respective to NAD$^+$ (F and H) to represent CD38 activity in plasma from WT, *mdx*, and MTBD/*mdx* mice at baseline or after social defeat stress. In panel (F): *& denotes $P < 0.05$ compared to baseline WT, baseline *mdx,* baseline MTBD/*mdx*, and WT post-SD; *^denotes $P < 0.05$ compared to baseline MTBD/*mdx* (interaction: $P = 0.045$). Bar graphs depict mean values (±SEM) from n = 4–8 mice/group. Comparisons between groups were made using two-way ANOVA with Tukey's multiple comparisons test (*$P < 0.05$; **$P < 0.01$; ***$P < 0.001$; ***$P < 0.0001$).

cultured myotubes shows that PGC-1α overexpression modulates the KYNA shunt of the KYN pathway in a muscle fiber-specific manner [22], suggesting that KYNA shunt dysregulation in *mdx* SkM is largely driven by dystrophin-deficient muscle fibers within the SkM compartment. Notably, MTBD/*mdx* mice, which express a full-length dystrophin/utrophin chimera in SkM and do not display post-scruff inactivity, exhibited a WT-like KYNA/KYN ratio and *Ppargc1a* transcript level (Figs 5C, F and 6A), further indicating that SkM dystrophinopathy drives KYNA shunt dysfunction. Our data reveal an association between scruff exposure, elevated SkM *Ppargc1a* transcript abundance, and increased KYNA shunt function in WT mice that is blunted in *mdx* mice (Figs 1C–F and 5A, B), suggesting a regulatory role for the KYNA shunt in stress resilience or vulnerability. However, enhanced

SkM KAT expression and PGC-1α transcriptional co-regulatory activity in the PGC-*mdx* mouse model did not result in protection against *mdx* scruff-induced inactivity. In addition to KYN pathway dysfunction, dystrophin-deficient *mdx* mice also demonstrated altered NAD$^+$ metabolism that may impact *mdx* stress physiology.

KYN pathway dysfunction has been proposed as a key mediator of numerous pathologies with an inflammatory component, including behavioral maladaptations to stress [26, 49], depression and mood disorders [50], age-related sarcopenia [51, 52], and cancer [53]. Our results from pharmacological and genetic manipulation of the extrahepatic KYN pathway suggest that, contrary to expectations, KYN pathway hyperactivity does not play a central role in the exaggerated acute stress response of *mdx* mice, acute stress response of *mdx* mice, although we did
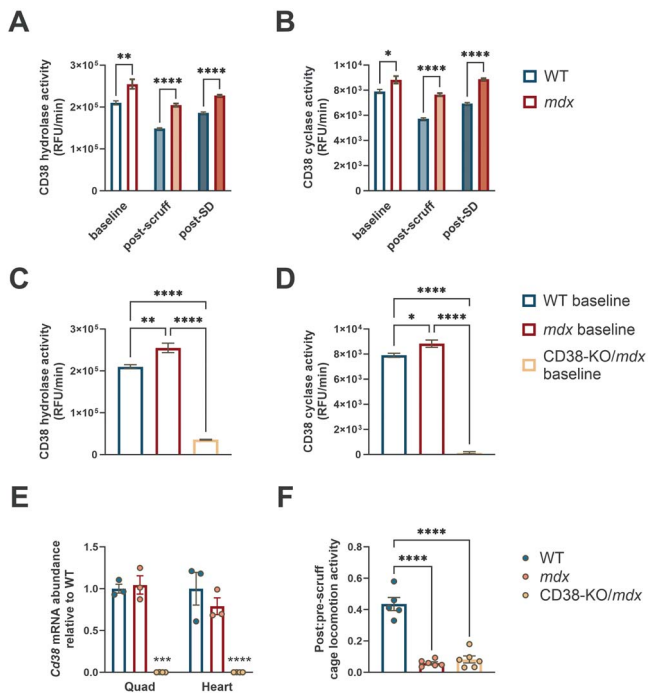
**Figure 9.** CD38 metabolism is elevated in *mdx* SkM, but does not mediate *mdx* scruff-dependent inactivity. (A and B) Fluorescence-based CD38 dual enzymatic activity analysis of CD38 hydrolase (A) and cyclase (B) activity in WT and *mdx* quadriceps muscle at baseline (n = 5 mice/group), 30 min after scruff exposure (n = 5–6 mice/group), or after social defeat stress (n = 3–4 mice/group). (C and D) Baseline CD38 enzymatic activity analysis of CD38 hydrolase (C) and cyclase (D) activity in WT, *mdx*, and CD38-KO/*mdx* quadriceps muscle (n = 5 mice/group). (E) qRT-PCR analysis of *Cd38* mRNA abundance in WT (n = 3 mice), *mdx* (n = 3 mice), and CD38-KO/*mdx* (n = 4 mice) quadriceps and cardiac muscle. (F) Ratio of open field horizontal locomotion distance for 30 min before and after a 30 s scruff exposure in WT, *mdx*, and CD38-KO/*mdx* mice. Bar graphs depict mean values (±SEM). Comparisons between groups in (A and B) were made using unpaired t-tests. Comparisons between groups in (C–F) were made using one-way ANOVA with Tukey's multiple comparisons test (*$P < 0.05$; **$P < 0.01$; ***$P < 0.001$; ***$P < 0.0001$).

not test KYN metabolic regulation over a longer post-stress time course or in response to prolonged CSS. Moreover, we demonstrate that the manifold benefits of PGC-1$\alpha$ overexpression to *mdx* SkM function—for example, improved mitochondrial biogenesis, enhanced utrophin expression, increased oxidative capacity, and reduced susceptibility to contraction-induced injury [35, 40, 41, 54]—are not sufficient to improve scruff-induced inactivity. We have previously established that utrophin overexpression in Fiona/*mdx* SkM is protective against stress susceptibility [13], (Fig. 6E). Here we demonstrate that the level of SkM utrophin overexpression is crucial for *mdx* stress resilience, since PGC/*mdx* that do not upregulate SkM utrophin to the same level as Fiona/*mdx* (Fig. 6F) remain inactive after scruff exposure (Fig. 6E). Our data is consistent with the finding that rescuing the primary *mdx* defect by repletion of full-length dystrophin or utrophin in SkM is protective against *mdx* stress pathology [13]. In light of the protection conferred by SkM PGC-1$\alpha$ overexpression against chronic stress-induced depression in WT mice [22], our data suggests that scruff-induced inactivity in *mdx* mice occurs via a mechanism that is distinct from the depressive or anxiety-like behavioral responses mediated by chronic inflammation and KYN pathway neurotoxicity. Further experimentation is required to determine whether global IDO1 ablation or KYNA shunt restoration via PGC-1$\alpha$ overexpression in SkM prevent *mdx* hypotension and

lethality responses to CSS, which involves sustained hypotension in moribund *mdx* mice [13] and triggers depressive behavior in WT mice [55]. Genetic modulation of KYN pathway activity to reduce circulating vasodilatory and neurotoxic KYN intermediates may improve both WT and *mdx* pathological responses to the acute phase of CSS.

Our investigation focused on metabolic alterations in *mdx* mice that are hypothesized to originate with chronic inflammation caused by asynchronous cycles of dystrophin-deficient muscle degeneration and repair. The experiments performed to address this hypothesis also provided clues as to whether inflammation itself, upstream of its effects on metabolic function, is key to *mdx* stress pathology. PGC/*mdx* mice restore the KYNA shunt of the KYN pathway in SkM, while CD38-KO/*mdx* mice prevent CD38 hyperactivity and restore NAD+ globally, and both genetic models also ameliorate muscle fiber injury and inflammation in *mdx* mice [35, 41, 43]. Neither PGC/*mdx* nor CD38-KO/*mdx* mice were protected from exaggerated scruff inactivity (Figs 6E and 9F), suggesting that KYN or NAD+ metabolic dysfunction and inflammation alone are insufficient to explain *mdx* stress susceptibility. In contrast, stress protection in MTBD/*mdx* and Fiona/*mdx* mice that transgenically replete dystrophin/utrophin—and consequently exhibit reduced SkM injury and inflammation (Fig. 6E) [13]—indicates that utrophin or dystrophin repletion, rather than reduced inflammation alone, is key to rescuing *mdx* stress pathology. Our findings do not exclude a role for inflammation in the *mdx* stress response mechanism, but do suggest the involvement of additional dystrophin-dependent contributors that remain to be identified.

An unexpected finding from our *mdx* KYN pathway investigation was that the terminal KYN pathway metabolite and substrate for the *de novo* NAD+ synthesis pathway, QA, is reduced in *mdx* circulation (Fig. 3G and H). Reduced plasma QA levels may be explained by reduced extrahepatic KYN metabolic flux in muscle, immune cells, or other KYN enzyme-expressing tissues, as well as by increased QA tissue uptake from circulation. The metabolomics methods used in this study involve targeted quantification of specified pathway metabolites from a limited number of tissues collected at a single time point. Our methodologies preclude us from making conclusions about tissue origins of metabolite production, metabolic inter-organ exchange, alterations in central carbon metabolism that regulates NAD+ levels, or metabolic pathway flux over the course of a stress exposure and recovery. However, the known defect in *mdx* NAD+ SkM metabolism [42–44], as well as the observation that NAD+ and QA levels are recovered in MTBD/*mdx* mice that differ from *mdx* mice specifically in the expression of SkM dystrophin, provide a compelling case for the contribution of SkM to *mdx* KYN and NAD+ metabolic dysfunction.

We demonstrated that NAD+ levels are reduced in *mdx* SkM and the NAD+/NADH redox pair is shifted toward a more reduced state at baseline, while the NAD+/NADH ratio is reduced in both healthy and *mdx* SkM after a psychosocial stress exposure (Fig. 7B–D). However, MTBD/*mdx* mice also exhibit a reduced NAD+/NADH ratio at baseline (Fig. 7D), which suggests that NAD+ redox balance may not be entirely dependent upon SkM dystrophin expression or influence stress susceptibility. Circulating NAD+ levels are reduced independent of genotype after SD stress (Fig. 8A). These data align with the observation that circulating QA levels are reduced independent of genotype after SD stress exposure and suggests a dystrophinopathy-independent mechanism for NAD+ depletion after stress that may rely on reduced KYN pathway flux through *de novo* NAD+ synthesis.

NAD+ salvage pathway metabolism appears largely unaltered between healthy and *mdx* SkM, while salvage pathway metabolites NR and NAM, but not NMN, are elevated in *mdx* and MTBD/*mdx* circulation independent of stress exposure (Fig. 8B–D). NMN is a direct NAD+ precursor, whereas NR and NAM must be metabolized to NMN to regenerate NAD+. Unchanged levels of NMN in *mdx* SkM and circulation (Figs 7F and 8D), along with reduced NAD+ content (Fig. 7B) and elevated circulating salvage pathway precursor abundance (Fig. 8B and C), suggests a potential blockade in *mdx* NAD+ salvage pathway flux at the level of NR and NAM. Indeed, the enzymes that convert NR and NAM to NMN, nicotinamide riboside kinases 1 and 2 (NRK1/2) and nicotinamide phosphoribosyltransferase (NAMPT), respectively, were previously shown to be transcriptionally downregulated in *mdx* SkM [42, 43]. NAMPT, which is a rate-limiting salvage pathway enzyme, was also reduced at the transcript level in human DMD SkM biopsies and at the protein level in *mdx* muscle [42]. In contrast, NMN-converting enzymes NMN adenylyltransferases (NMNATs) were transcriptionally upregulated in *mdx* SkM, but protein levels of NMNATs were unchanged between WT and *mdx* muscle [42]. These data supports a blockade in *mdx* salvage pathway metabolism at the step of NR/NAM conversion to NMN and may explain the underwhelming performance of NR supplementation as a therapeutic strategy for recovering *mdx* NAD+ levels and muscle function [45, 46, 56].

NAD+ deficits in *mdx* SkM do not appear to be adequately explained by reduced salvage pathway flux, because both *mdx* and MTBD/*mdx* mice exhibited elevated circulating NAM and NR levels (Fig. 8B and C), whereas NAD+ content was repleted in MTBD/*mdx* SkM (Fig. 7B). An alternative route for NAD+ depletion is through catabolism by poly (ADP-ribose) polymerases (PARPs), sirtuins, and CD38, which generate NAM as a byproduct. CD38 produces NAM as well as ADPR and cADPR, 2 s messenger metabolites that regulate intracellular calcium flux and are elevated by inflammatory cytokines under pathological conditions such as airway hyper-responsiveness, diet-induced obesity, and age-related disease [57, 58]. Cytokine-induced CD38 hyperactivity in dystrophin-deficient muscle is thus a potential contributor to NAD+ defects and calcium handling dysregulation in *mdx* mice. Indeed, recent reports have suggested that CD38 pharmacological blockade and genetic ablation are more effective than NR as an NAD+-repletion strategy in *mdx* skeletal and cardiac muscle [43, 45]. Global CD38 genetic ablation in *mdx* mice has also been shown to improve muscle function, reduce fibrosis, and prevent *mdx* lethality in response to pharmacological β-adrenergic receptor (β-AR) agonism with isoproterenol [43]. The protective effects of CD38 ablation against pharmacological stress have been attributed to restored cardiomyocyte calcium homeostasis and reduced ryanodine receptor opening that triggers arrhythmogenic calcium (Ca2+) sparks in response to β-AR agonist treatment in *mdx* mice [43].

Our targeted metabolomics data suggests that CD38 catabolic activity is upregulated in *mdx* mice after psychosocial stress, as indicated by an elevated ADPR/NAD+ ratio in SkM and plasma from SD-exposed *mdx* mice (Figs 7H and 8E). CD38 is a multifunctional enzyme that possesses both ADP-ribosyl cyclase and cADPR hydrolase activity to produce cADPR and ADPR, respectively [58]. An orthogonal fluorescence-based approach to measure dual CD38 enzymatic activity [48] supported our metabolomics data and revealed both elevated CD38 hydrolase and cyclase activity in *mdx* SkM at baseline and after graded forms of physiological stress exposure (Fig. 9A–D).

CD38 hyperactivity in dystrophin-deficient muscle compartments may be key to the regulation of intramuscular NAD+ content, β-AR agonist-induced cardiac arrhythmias, and *mdx* muscle function by CD38. Although we did not assess NAD+ metabolic alterations in the *mdx* heart, the trend toward increased ADPR/NAD+ that is present in both SkM and plasma suggests that ADPR and/or cADPR could be secreted into the circulation by SkM and taken up by the heart to influence cardiac second messenger levels and Ca2+ influx into cardiomyocytes. Additionally, CD38 inhibition has been shown to ameliorate *mdx* alterations in glycolytic and pentose phosphate pathway metabolism [45], suggesting that CD38 pathway dysfunction has a broader impact on central metabolism in *mdx* skeletal and cardiac muscle that may impact *mdx* muscle function.

In light of our finding that CD38 metabolism is uniquely altered in *mdx* mice after psychosocial stress, we investigated the potential for CD38 genetic ablation to protect against *mdx* stress pathology and did not observe amelioration of scruff-induced inactivity in the CD38-KO/*mdx* mouse model (Fig. 9F). The beneficial effects of CD38 ablation on *mdx* skeletal, cardiac, and respiratory muscle function and histopathology, as well as the protection against isoproterenol-induced lethality [43], indicates that CD38 plays an important role in regulating DMD disease progression through a mechanism that is independent from the pathway that influences *mdx* stress pathology. Our previous work demonstrated correction of *mdx* stress pathology without cardiac protection [13], and retention of CD38-KO/*mdx* stress pathology in the current work suggests that improved Ca2+ regulation, cardiac improvements, and reduced arrhythmia susceptibility are insufficient to rescue *mdx* vulnerability to scruff stress.

## Conclusions

The KYN pathway is gaining notoriety as a biomarker for and modulator of exercise adaptations, as well as a mediator of pathological stress response in a pro-inflammatory context [28, 31, 33]. Despite evidence that *mdx* SkM exhibits a deficit in neurotoxic KYN disposal through the KYNA shunt, our data do not demonstrate a protective role for rescuing the SkM KYNA shunt or ablating extrahepatic KYN pathway activity in *mdx* mice acutely exposed to stressful scruff handling. CD38 has recently received attention for its contributions to cardiac and SkM NAD+ deficits, Ca2+ dysregulation, oxidative stress, and muscle frailty in DMD and aging contexts [43, 45, 59]. We confirmed a defect in *mdx* NAD+ metabolism and show that *mdx* mice exhibit elevated CD38-NAD+-ase activity at baseline and after stress exposure. However, global CD38 ablation did not prevent scruff-induced inactivity in *mdx* mice, suggesting that CD38-mediated cardiac and SkM NAD+ deficiency and Ca2+ dysregulation are not central to *mdx* physiological stress susceptibility. Exploration of alternative metabolic and signaling pathways that mediate inter-organ crosstalk in a physiological stress context will provide new insights into the mechanism underlying *mdx* stress pathology.

## Materials and methods
### Mice

All mice used in this study were adult males (3–4 months of age). Animal care and experimental procedures were approved by the Institutional Animal Care and Use Committee (IACUC) of the University of Minnesota. C57BL10/J mice used as wild-type controls and C57BL/10ScSn-*Dmd*^*mdx*/J (*mdx*) mice were

bred in-house or purchased from The Jackson Laboratory. The MTBD/*mdx* transgenic mouse line expressing a human skeletal actin promotor-driven full-length dystrophin/utrophin chimera with microtubule-binding spectrin repeats 20–24 of dystrophin replaced by non-binding repeats 18–22 of utrophin was generated previously [60] and bred in-house. The Fiona/*mdx* transgenic mouse line expressing a human skeletal actin promotor-driven full-length utrophin transgene was generated previously [61] and bred in-house. Skeletal muscle-specific PGC-1$\alpha$ transgenic mice (MCK-PGC-1$\alpha$) with PGC-1$\alpha$ overexpression driven by the Cre promotor [40] were generously provided by Glenn Rowe at the University of Alabama [35] and backcrossed onto the *mdx* background in our colony to generate PGC/*mdx* mice. Mice from the B6.129-*Ido1*$^{tm1Alm}$/J strain (IDO KO; JAX stock #005867) [62] with beta-galactosidase and neomycin resistance genes substituted for exons 3–5 encoding the enzyme catalytic site in IDO1 were purchased from The Jackson Laboratory and backcrossed onto the *mdx* background to generate IDO-KO/*mdx* mice. CD38-KO mice with global CD38 enzyme ablation were generously provided by Alonso Guedes at the University of Minnesota [58] and backcrossed onto the *mdx* background in our colony to generate CD38-KO/*mdx* mice. Mice were group housed following standard specific pathogen free (SPF) procedures with *ad libitum* access to food and water on a 12-h light/dark cycle. Male CD1 mice that were used in the social defeat stress protocol as aggressive resident mice were purchased from Charles River Laboratories and individually housed in cages with the same general environmental conditions as described above.

## Scruff-induced inactivity

Activity was monitored using the SuperFlex Open Field activity monitoring system with AccuScan Fusion software (Version 3.4) by Omnitech Electronics, Inc. Activity was determined by total locomotion distance, measured by infrared beam breaks. Mice were individually placed in open-field cages for 30 min to record baseline locomotor activity, then were removed from the open-field cage and scruffed for 30 s by grasping the mouse by the nape of its neck and placing the tail between the palm of the hand and the 5$^{th}$ digit. Immediately following completion of the scruff, mice were placed back into the open-field cage and activity was monitored for an additional 30 min. Data are presented as total pre- and post-scruff locomotor activity or as a ratio of post:pre-scruff locomotor activity. After completing 30 min post-scruff activity cage monitoring, mice were anesthetized using tribromoethanol (Avertin) and euthanized via cervical dislocation. Skeletal muscle and plasma from blood obtained via cardiac puncture were collected for downstream biochemical analysis.

## 6 hour social defeat (SD) stress

The SD stress protocol was modified from our established protocol as an abbreviated and acute form of CSS [6, 13, 55]. Experimental mice were placed into the home cage of an aggressive resident CD1 mouse and exposed to a 10-min social defeat episode by the CD1 mouse. Experimental mice and resident CD1 mice were then separated with a cage divider and kept in sensory contact without physical interaction for 6 h, then experimental mice were euthanized via $CO_2$ and cervical dislocation. Skeletal muscle and plasma from trunk blood were collected for downstream biochemical analysis.

## Pharmacological pre-scruff treatment

Dystrophin-deficient *mdx* mice were randomized to receive sterilized saline (0.9% (w/v) NaCl in PBS) or IDO1 inhibitor 1-*L*-methyltryptophan (80 mg/kg) via intraperitoneal injection 1 h prior to performing a scruff stress assay as described above. WT mice were treated with saline as a control group and experimenters were blinded to treatment group. Mice were sacrificed at the experimental endpoint.

## Real-time quantitative PCR

Skeletal muscle, spleen, and lung tissue was ground to a powder using mortar and pestle in liquid nitrogen and further homogenized with mechanical disruption in Trizol reagent (15596-018, Thermo Fisher). RNA was extracted using the RNeasy Mini Kit (74104, Qiagen). Total RNA concentration and purity were determined using $A_{260/280}$ absorbance with a nanodrop spectrophotometer (Thermo Scientific). A standardized amount of RNA was reverse-transcribed to cDNA with the iScript Advanced cDNA Synthesis Kit (172-5038, Bio-Rad Laboratories), then cDNA was amplified using the SsoAdvanced Universal SYBR Green Supermix (172-5272, Bio-Rad Laboratories) on the C1000 Touch Thermal Cycler (Bio-Rad). RNA was amplified using primers specific to each gene of interest, detailed in Table S1. Housekeeping gene HPRT was used for relative quantification of mRNA transcript abundance. Data was analyzed using the CFX Manager 3.1 software (Bio-Rad).

## Western blotting

Quad muscle was homogenized using mortar and pestle in liquid nitrogen. Crushed tissue was lysed with 1% sodium dodecyl sulfate in 1xPBS with added protease inhibitors (100 nM Aprotonin, 10 mg/ml E-64, 100 $\mu$M Leupeptin, 1 mM PMSF, 1 $\mu$g/ml Pepstatin, 0.79 mg/ml Benzamidine). Lysates were clarified by centrifugation, then protein content was assessed by $A_{280}$ absorbance and samples were diluted to 2 mg/ml with PBS and $\beta$-mercaptoethanol for protein denaturation. Forty $\mu$g total protein was loaded on a 10% (KYN pathway enzyme blotting) or 3%–12% (utrophin blotting) polyacrylamide gel for 1.25 h at 150 V. Protein was transferred to a 0.45 $\mu$m polyvinylidene fluoride membrane (Immobilon-FL IPFL00010, Millipore Sigma) for 1 h at 0.8 A. Membranes were blocked with 5% nonfat milk in PBS for 1 h before overnight incubation with primary antibodies at 4°C. Primary antibodies included 1:10 000 *anti*-GAPDH (mouse: G8795; rabbit: G9545; Sigma-Aldrich) used as a membrane loading control; 1:1000 *anti*-CCBL1/KAT1 (12156-1-AP, Proteintech); 1:1000 *anti*-CCBL2/KAT3 (MBS3205107, MyBioSource); 1:1000 GOT2/KAT4 (14800-1-AP, Proteintech); 1:1000 *anti*-IDO1 (13268-1-AP, Proteintech); 1:1000 *anti*-KMO (60029-1-Ig, Proteintech); and 1:50 *anti*-utrophin (MANCHO3[8A4], DSHB). Secondary antibodies DyLight 680 and 800 (1:10 000, Cell Signaling) were incubated in the dark for 1 h at room temperature. Membranes were imaged and densitometry quantifications were made with a Licor Odyssey Infrared Imaging System and Image Studio Lite (5.x CLx/DLx) software.

## Targeted metabolomics mass spectrometry

We performed two customized MRM LC-MS/MS metabolomics experiments in collaboration with the University of Minnesota Center for Metabolomics and Proteomics (CMSP) with modifications from previous work [36, 37, 63, 64]. Experiment 1 included

WT, *mdx*, and MTBD/*mdx* plasma samples collected at baseline or after a scruff protocol, while Experiment 2 included WT, *mdx*, and MTBD/*mdx* plasma and quad samples collected at baseline or after a social defeat stress protocol.

## Experiment 1

Plasma samples were collected from WT, *mdx*, and MTBD/*mdx* mice at baseline or 30 min after scruff exposure, then samples were stored at −80°C until MS analysis. 25 $\mu$l plasma samples (n = 5 mice per group), as well as pooled quality control samples, were mixed with 7.5 $\mu$l deuterated (*d*-) internal standard mix (Trp-*d*5, 600 pg/$\mu$l; KYN-*d*4, 100 pg/$\mu$l; QUIN-*d*3, 50 pg/$\mu$l; PIC-*d*4, 100 pg/$\mu$l; KYNA-*d*5, 0.2 pg/$\mu$l) and 25 $\mu$l 0.2% (v/v) formic acid in MS-grade water (acidified mobile phase). Sample mixtures were pipetted in triplicate into flat-bottom 96-well plates, followed by 375 $\mu$l methanol, then the plate was sealed and briefly centrifuged at 3000 × g. The plate was placed at −20°C for 30 min to allow protein precipitation, then was centrifuged at 3000 × g (4°C for 15 min) before supernatants were transferred to low-binding 1.5 ml centrifuge tubes. Samples were dried under nitrogen and resuspended in 50 $\mu$l acidified mobile phase. Unlabeled metabolite standards were mixed and serially diluted, then 15 ng/ml internal standard mix was added to each standard dilution to construct a calibration curve with concentration ranges optimized for each endogenous metabolite based on preliminary experiments.

Samples and standards (10 $\mu$l) were injected in duplicate in randomized order and were chromatographically separated using an Agilent 1290 Infinity II LC equipped with a Phenomenex Kinetex C18 100 Å (150 × 2.1 mm, 2.6 $\mu$m; 00F-4462-AN) analytical column. Autosampler temperature was set to 4°C and the column temperature was 55°C. Metabolites were eluted from the column using a solvent gradient of two mobile phases. Mobile phase A consisted of 0.2% (v/v) formic acid in water and mobile phase B consisted of 95% (v/v) acetonitrile and 5% (v/v) water with 0.2% (v/v) formic acid. The flow rate was set to 0.4 ml/min, with a 9 min total method runtime. The mobile phase gradient started with 100% mobile phase A for 3 min, followed by 90% A/10% B for 2 min, 5% A/95% B for 1 min, and 100% A for 2 min. Metabolites were detected using an Agilent 6495C triple quadrupole MS with an Agilent Jet Stream electrospray ion source operating in positive ionization mode. MS parameters are as follows: ion dwell time, 10 ms; fragmentor energy, 166 V; cell accelerator voltage, 5 V; capillary, 3500 V; nozzle voltage, 500 V; iFunnel high pressure RF, 150 V; iFunnel low pressure RF, 60 V; gas temperature, 290°C; gas flow, 17 l/min; nebulizer pressure, 25 psi; sheath gas temperate, 350°C; and sheath gas flow, 12 l/min. MRM acquisition parameters and mass-to-charge ratio transitions, along with limits of quantification (LOQ) for each metabolite, are reported in Table S2.

Total ion chromatograms were extracted and analyzed using Agilent MassHunter software. Extracted ion chromatogram area under the curve (AUC) was integrated using automatic baseline correction for each MRM transition. KYN metabolites in a sample were quantified by dividing the metabolite AUC by the AUC of its respective labeled internal standard, followed by interpolation to a calibration curve prepared fresh and injected in triplicate at the beginning, middle, and end of the experimental run. For metabolites without labeled internal standards, an internal standard with similar chemical composition and chromatographic profile was used. Dilution corrections and molarity conversions were calculated, and data are presented as bar graphs to compare metabolite levels between different genotypes and stress treatment conditions.

## Experiment 2

Plasma and quad SkM samples (n = 4–7 per group) were collected from WT, *mdx*, and MTBD/*mdx* mice at baseline or 6 h post-SD exposure. Quad muscles were flash frozen in liquid nitrogen, then both plasma and SkM samples were stored at −80°C until MS analysis. 40 $\mu$l plasma samples and pooled quality control samples were mixed with 45 $\mu$l mobile phase A (5 mM ammonium acetate, 5 $\mu$M medronic acid in water, pH 3.0) and 20 $\mu$l internal standard mix (Trp-*d*5, 30 ng/$\mu$l; KYN-*d*4, 100 pg/$\mu$l; QUIN-*d*3, 250 pg/$\mu$l; PIC-*d*4, 60 pg/$\mu$l; KYNA-*d*5, 500 pg/$\mu$l; $^{13}C_2$,$^{15}$N-3-HK, 100 pg/$\mu$l; $^{13}C_5$-cyclic adenosine monophosphate, 4 pg/$\mu$l; NAM-*d*4, 100 pg/ul; $^{15}N_5$-adenosine monophosphate, 150 pg/$\mu$l). Sample mixtures were loaded in duplicate onto Ostro Protein Precipitation and Phospholipid Removal Plates (186005518, Waters), then 150 $\mu$l acetonitrile with 0.1% (v/v) formic acid was added to each well and the Ostro plate was vortexed briefly. Samples were eluted from the Ostro plate following the manufacturer protocol with a vacuum manifold (186001831, Waters). Samples were dried using a vacuum centrifuge and resuspended in 30 $\mu$l mobile phase A, then were vortexed for 5 min and briefly centrifuged with the supernatant used for undiluted and 1:10 diluted sample injections. 50–100 mg quad samples were added to 85% ethanol, 15% 0.01 M phosphate buffer in a 3:1 solvent-to-tissue ratio. SkM samples were homogenized using a bead blender (4116-BBY24M, Next Advance) set at maximum speed for 10 min, then samples were centrifuged at 14 000 × g, 4°C for 15 min. Two 90 $\mu$l aliquots were obtained from each sample supernatant for duplicate measurements, then 10 $\mu$l internal standard mix was added (Trp-*d*5, 20 ng/$\mu$l; KYN-*d*4, 40 pg/$\mu$l; QA-*d*3, 100 pg/$\mu$l; PA-*d*4, 40 pg/$\mu$l; KYNA-*d*5, 50 pg/$\mu$l; $^{13}C_2$,$^{15}$N-3-HK, 250 pg/$\mu$l; $^{13}C_5$-cyclic adenosine monophosphate, 5 pg/$\mu$l; NAM-*d*4, 18 ng/ul; $^{15}N_5$-adenosine monophosphate, 150 pg/$\mu$l). Samples were dried using vacuum centrifugation and resuspended in 30 $\mu$l mobile phase A, then were vortexed, centrifuged, and diluted as for plasma samples. Calibration standards were prepared as in Experiment 1 with internal standard mix corresponding to plasma or skeletal muscle experimental analysis.

Standards, undiluted samples, and 1:10 diluted samples (10 $\mu$l) were injected in duplicate in randomized order and were chromatographically separated using a Shimadzu UFLC XR (L20304924701 and L20434950623) equipped with an Agilent InfinityLab Poroshell 120 EC-C18 (3.0 × 150 mm, 2.7 $\mu$m) analytical column. Autosampler temperature was set to 4°C and column temperature was 50°C. Metabolites were eluted from the column using a solvent gradient of two mobile phases. Mobile phase A consisted of 5 mM ammonium acetate, 5 $\mu$M medronic acid in water, pH 3.0, and mobile phase B consisted of methanol with 5 $\mu$M medronic acid. The flow rate was set to 0.15 ml/min, with a 15 min total method runtime. The mobile phase gradient started with 98% A/2% B for 11 min, followed by 100%B for 1.5 min, 98% A/2% B for 0.5 min, and 100% A for 2 min. Metabolites were detected using a SCIEX 5500 triple quadrupole/linear ion trap MS with a Turbo V electrospray ion source operating in positive ionization mode. MS parameters are as follows: ion dwell time, 10 ms; fragmentor energy, 166 V; cell accelerator voltage, 4 V; IonSpray voltage, 4500 V; curtain gas flow, 35 l/min; collision gas flow, medium; ion source gas temperature, 500°C; ion source gas 1 flow, 60 l/min; ion source gas 2 flow, 70 l/min. MRM acquisition parameters and mass-to-charge ratio transitions, as well as LOQ for each metabolite, are reported in Table S2. Total ion chromatograms were extracted and analyzed using SCIEX MultiQuant software. Data were analyzed as for Experiment 1.

## CD38 enzymatic activity assay

CD38 NAD$^+$-ase hydrolase and cyclase activity were measured as previously described [48] for WT, *mdx*, and CD38-KO/*mdx* quadriceps muscle obtained at baseline and after scruff and 6 h SD exposure. Briefly, 30–60 mg quadriceps muscle was homogenized using mortar and pestle with liquid nitrogen, then lysed in sucrose buffer (0.25 M sucrose, 40 mM Tris-HCl, pH 7.4) with sonication and diluted in sucrose buffer to normalize protein concentration. To 50 $\mu$g protein samples in duplicate, 50 $\mu$M nicotinamide 1, N6-ethenoadenine dinucleotide (sc-215559; Santa Cruz Biotechnology) or 200 $\mu$M nicotinamide guanine dinucleotide (N5131; Sigma-Aldrich) were added as NAD$^+$ analog substrates to measure CD38 hydrolase and cyclase activity, respectively. Recombinant human CD38 (2404-AC-010; R&D Systems) was tested alongside samples as a positive control, and matrix and substrate blanks were included. Fluorescent product formation was measured using a SpectraMax$^®$ iD3 Multi-Mode Microplate Reader (Molecular Devices) with an emission wavelength of 300 nm and an excitation wavelength of 410 nm. A kinetic analysis was performed for 1.5 h, with readings every 50 s. Average fluorescent values for each sample group were blank-corrected and plotted against time in X-Y plots to obtain slopes $\pm$ SEM of enzymatic activity curves as readouts of CD38 hydrolase and cyclase activity.

## Chemicals

Pharmacological agent 1-*L*-methyltryptophan was purchased from Sigma-Aldrich (447439). Unlabeled chemical standards used for LC/MS analysis were purchased from Sigma: *L*-tryptophan (1700501), *L*-kynurenine (K8625), *L*-kynurenic acid (K3375), *DL*-3-hydroxykynurenine (H1771), quinolinic acid (2,3-pyridinedicarboxylic acid; P63204), 2-picolinic acid (P42800), 3-hydroxyanthranilic acid (148776), xanthurenic acid (D120804), $\beta$-nicotinamide adenine dinucleotide phosphate sodium salt hydrate (N0505), $\beta$-nicotinamide adenine dinucleotide 2′-phosphate reduced tetrasodium salt hydrate (N7505), $\beta$-nicotinamide mononucleotide (N3501), nicotinic acid (47864), nicotinamide (72340), nicotinic acid mononucleotide (N7764), nicotinic acid-adenine dinucleotide (N4256), nicotinamide riboside chloride (SMB00907), adenosine 5′-diphosphoribose sodium salt (A0752), and adenosine 3′,5′-cyclic monophosphate sodium salt monohydrate (A6885). Deuterium (*d*-), $^{13}$C-, or $^{15}$N- heavy isotope labeled standards were obtained from the following vendors: *L*-tryptophan-*d*5 (34829; Cayman Chemical), *L*-kynurenine-*d*4 (36307; Cayman Chemical), quinolinic acid-*d*3 (P991633; Toronto Research Chemicals), 2-picolinic acid-*d*4 (615757; Sigma-Aldrich), kynurenic acid-*d*5 (K660502; Toronto Research Chemicals), nicotinamide-*d*4 (DLM-6883; Cambridge Isotope Laboratories), adenosine-$^{15}$N$_5$ 5′-monophosphate sodium salt (662658; Sigma-Aldrich), and $^{13}$C$_5$-cyclic adenosine monophosphate (A280457; Toronto Research Chemicals). LC-MS reagents were purchased from Sigma: methanol (34860), acetonitrile (34998), formic acid (695076), MS-grade water (1.15333), medronic acid (M0240000), and ammonium acetate (5330040050). Sucrose (S0389-1 kg) and Trizma$^®$ base (T6066) were obtained from Sigma-Aldrich.

## Statistical methods

All statistics were performed with GraphPad Prism, version 10.1.0. Outlier calculations were made using Grubb's test on each quantitative data set. For comparisons between two independent groups, an unpaired t-test was performed. For comparisons between at least three groups and a single condition, a one-way ANOVA statistical test was performed. For comparisons involving two factors, a two-way ANOVA statistical test was performed. For significant interaction terms, ANOVA tests were followed by a Tukey's multiple comparisons post-hoc statistical test. For survival comparisons between two or more groups, Kaplan-Meier survival curve analysis was performed and statistical comparison between curves was performed with the log-rank (Mantel-Cox) test and Gehan-Breslow-Wilcoxon test. Values are expressed as mean $\pm$ SEM, and significance is presented as *$P < 0.05$, **$P < 0.01$, ***$P < 0.001$, and ****$P < 0.0001$.

## Author contributions

E.J. and J.M.E. conceived the study and designed experiments; E.J., W.M.S., B.D., B.S., and M.R. performed experiments; M.R. and A.B. provided reagents and tools for stress physiology experiments; E.J. analyzed data and wrote the manuscript; E.J. and J.M.E. made manuscript revisions.

## Supplementary data

Supplementary data is available at *HMG Journal* online.

*Conflict of interest statement:* The authors do not have any conflicts of interest to declare.

## References

1. Broomfield J, Hill M, Guglieri M. *et al.* Life expectancy in Duchenne muscular dystrophy: reproduced individual patient data meta-analysis. *Neurology* 2021;**97**:e2304–14.

2. Cotton S, Voudouris NJ, Greenwood KM. Intelligence and Duchenne muscular dystrophy: full-scale, verbal, and performance intelligence quotients. *Dev Med Child Neurol* 2001;**43**: 497–501.

3. Snow WM, Anderson JE, Jakobson LS. Neuropsychological and neurobehavioral functioning in Duchenne muscular dystrophy: a review. *Neurosci Biobehav Rev* 2013;**37**:743–52.

4. Maresh K, Papageorgiou A, Ridout D. *et al.* Startle responses in Duchenne muscular dystrophy: a novel biomarker of brain dystrophin deficiency. *Brain* 2023;**146**:252–65.

5. Rosenberg AS, Puig M, Nagaraju K. *et al.* Immune-mediated pathology in Duchenne muscular dystrophy. *Sci Transl Med* 2015;**7**:299rv4.

6. Bartolomucci A, Palanza P, Sacerdote P. *et al.* Social factors and individual vulnerability to chronic stress exposure. *Neurosci Biobehav Rev* 2005;**29**:67–81.

7. Takahashi A, Flanigan ME, McEwen BS. *et al.* Aggression, social stress, and the immune system in humans and animal models. *Front Behav Neurosci* 2018;**12**:56.

8. Gough M, Godde K. A multifaceted analysis of social stressors and chronic inflammation. *SSM Popul Health* 2018;**6**:136–40.

9. Razzoli M, Nyuyki-Dufe K, Gurney A. *et al.* Social stress shortens lifespan in mice. *Aging Cell* 2018;**17**:e12778.

10. Bartolomucci A. Social stress, immune functions and disease in rodents. *Front Neuroendocrinol* 2007;**28**:28–49.

11. Powell ND, Sloan EK, Bailey MT. *et al.* Social stress up-regulates inflammatory gene expression in the leukocyte transcriptome via β-adrenergic induction of myelopoiesis. *Proc Natl Acad Sci U S A* 2013;**110**:16574–9.

12. Menard C, Pfau ML, Hodes GE. *et al.* Social stress induces neurovascular pathology promoting depression. *Nat Neurosci* 2017;**20**:1752–60.

13. Razzoli M, Lindsay A, Law M. *et al.* Social stress is lethal in the mdx model of Duchenne muscular dystrophy. *EBioMedicine* 2020;**55**:102700.

14. Goyenvalle A, Griffith G, Babbs A. *et al.* Functional correction in mouse models of muscular dystrophy using exon-skipping tricyclo-DNA oligomers. *Nat Med* 2015;**21**:270–5.

15. Saoudi A, Barberat S, le Coz O. *et al.* Partial restoration of brain dystrophin by tricyclo-DNA antisense oligonucleotides alleviates emotional deficits in mdx52 mice. *Mol Ther Nucleic Acids* 2023;**32**:173–88.

16. Sekiguchi M, Zushida K, Yoshida M. *et al.* A deficit of brain dystrophin impairs specific amygdala GABAergic transmission and enhances defensive behaviour in mice. *Brain* 2009;**132**:124–35.

17. Vigneron N, van Baren N, Van den Eynde BJ. Expression profile of the human IDO1 protein, a cancer drug target involved in tumoral immune resistance. *Oncoimmunology* 2015;**4**:e1003012.

18. Castro-Portuguez R, Sutphin GL. Kynurenine pathway, NAD+ synthesis, and mitochondrial function: targeting tryptophan metabolism to promote longevity and healthspan. *Exp Gerontol* 2020;**132**:110841.

19. Sakakibara K, Feng GG, Li J. *et al.* Kynurenine causes vasodilation and hypotension induced by activation of KCNQ-encoded voltage-dependent K+ channels. *J Pharmacol Sci* 2015;**129**:31–7.

20. Stanley CP, Maghzal GJ, Ayer A. *et al.* Singlet molecular oxygen regulates vascular tone and blood pressure in inflammation. *Nature* 2019;**566**:548–52.

21. González Esquivel D, Ramírez-Ortega D, Pineda B. *et al.* Kynurenine pathway metabolites and enzymes involved in redox reactions. *Neuropharmacology* 2017;**112**:331–45.

22. Agudelo LZ, Femenía T, Orhan F. *et al.* Skeletal muscle PGC-1α1 modulates kynurenine metabolism and mediates resilience to stress-induced depression. *Cell* 2014;**159**:33–45.

23. Wang B, Lian YJ, Su WJ. *et al.* HMGB1 mediates depressive behavior induced by chronic stress through activating the kynurenine pathway. *Brain Behav Immun* 2018;**72**:51–60.

24. Laugeray A, Launay JM, Callebert J. *et al.* Chronic treatment with the IDO1 inhibitor 1-methyl-D-tryptophan minimizes the behavioural and biochemical abnormalities induced by unpredictable chronic mild stress in mice—comparison with fluoxetine. *PLoS One* 2016;**11**:e0164337.

25. Schwarcz R, Stone TW. The kynurenine pathway and the brain: challenges, controversies and promises. *Neuropharmacology* 2017;**112**:237–47.

26. Kim Y-K, Jeon SW. Neuroinflammation and the immune-kynurenine pathway in anxiety disorders. *Curr Neuropharmacol* 2018;**16**:574–82.

27. Huang YS, Ogbechi J, Clanchy FI. *et al.* IDO and kynurenine metabolites in peripheral and CNS disorders. *Front Immunol* 2020;**11**:388.

28. Pedersen BK. Physical activity and muscle–brain crosstalk. *Nat Rev Endocrinol* 2019;**15**:383–92.

29. Savitz J. The kynurenine pathway: a finger in every pie. *Mol Psychiatry* 2020;**25**:131–47.

30. Badawy AAB. Kynurenine pathway and human systems. *Exp Gerontol* 2020;**129**:110770.

31. Agudelo LZ, Ferreira DMS, Dadvar S. *et al.* Skeletal muscle PGC-1α1 reroutes kynurenine metabolism to increase energy efficiency and fatigue-resistance. *Nat Commun* 2019;**10**:1–12.

32. Schlittler M, Goiny M, Agudelo LZ. *et al.* Endurance exercise increases skeletal muscle kynurenine aminotransferases and plasma kynurenic acid in humans. *Am J Physiol Cell Physiol* 2016;**310**:C836–40.

33. Cervenka I, Agudelo LZ, Ruas JL. Kynurenines: Tryptophan's metabolites in exercise, inflammation, and mental health. *Science* 2017;**357**:eaff9794.

34. Copeland EN, Watson CJF, Whitley KC. *et al.* Kynurenine metabolism is altered in mdx mice: a potential muscle to brain connection. *Exp Physiol* 2022;**107**:1029–36.

35. Chan MC, Rowe GC, Raghuram S. *et al.* Post-natal induction of PGC-1α protects against severe muscle dystrophy independently of utrophin. *Skelet Muscle* 2014;**4**:1–13.

36. Cuny H, Kristianto E, Hodson MP. *et al.* Simultaneous quantification of 26 NAD-related metabolites in plasma, blood, and liver tissue using UHPLC-MS/MS. *Anal Biochem* 2021;**633**:114409.

37. Fuertig R, Ceci A, Camus SM. *et al.* LC-MS/MS-based quantification of kynurenine metabolites, tryptophan, monoamines and neopterin in plasma, cerebrospinal fluid and brain. *Bioanalysis* 2016;**8**:1903–17.

38. Grobben Y, de Man J, van Doornmalen AM. *et al.* Targeting indoleamine 2,3-dioxygenase in cancer models using the novel small molecule inhibitor NTRC 3883-0. *Front Immunol* 2021;**11**:609490.

39. Wirthgen E, Otten W, Tuchscherer M. *et al.* Effects of 1-methyltryptophan on immune responses and the kynurenine pathway after lipopolysaccharide challenge in pigs. *Int J Mol Sci* 2018;**19**:3009–32. https://doi.org/10.3390/ijms19103009.

40. Handschin C, Kobayashi YM, Chin S. *et al.* PGC-1α regulates the neuromuscular junction program and ameliorates Duchenne muscular dystrophy. *Genes Dev* 2007;**21**:770–83.

41. Selsby JT, Morine KJ, Pendrak K. *et al.* Rescue of dystrophic skeletal muscle by PGC-1α involves a fast to slow Fiber type shift in the mdx mouse. *PLoS One* 2012;**7**:e30063.

42. Ryu D, Zhang H, Ropelle ER. *et al.* NAD+ repletion improves muscle function in muscular dystrophy and counters global parylation. *Sci Transl Med* 2016;**8**:1–15.

43. de Zélicourt A, Fayssoil A, Dakouane-Giudicelli M. *et al.* CD38-NADase is a new major contributor to Duchenne muscular dystrophic phenotype. *EMBO Mol Med* 2022;**14**:e12860.

44. Chalkiadaki A, Igarashi M, Nasamu AS. *et al.* Muscle-specific SIRT1 gain-of-function increases slow-twitch fibers and ameliorates pathophysiology in a mouse model of Duchenne muscular dystrophy. *PLoS Genet* 2014;**10**:e1004490.

45. Frederick DW, McDougal AV, Semenas M. *et al.* Complementary NAD+ replacement strategies fail to functionally protect dystrophin-deficient muscle. *Skelet Muscle* 2020;**10**:30.

46. Spaulding HR, Quindry T, Hammer K. *et al.* Nutraceutical and pharmaceutical cocktails did not improve muscle function or reduce histological damage in D2-mdx mice. *J Appl Physiol* 2019;**127**:1058–66.

47. Demarest TG, Truong GTD, Lovett J. *et al.* Assessment of NAD+ metabolism in human cell cultures, erythrocytes, cerebrospinal fluid and primate skeletal muscle. *Anal Biochem* 2019;**572**:1–8.

48. de Oliveira GC, Kanamori KS, Auxiliadora-Martins M. *et al.* Measuring CD38 hydrolase and cyclase activities: 1,N6-Ethenonicotinamide adenine dinucleotide ($\varepsilon$-NAD) and nicotinamide guanine dinucleotide (NGD) fluorescence-based methods. *Bio Protoc* 2018;**8**:e2938.

49. Fuertig R, Azzinnari D, Bergamini G. *et al.* Mouse chronic social stress increases blood and brain kynurenine pathway activity and fear behaviour: both effects are reversed by inhibition of indoleamine 2,3-dioxygenase. *Brain Behav Immun* 2016;**54**:59–72.

50. Kruse JL, Cho JHJ, Olmstead R. *et al.* Kynurenine metabolism and inflammation-induced depressed mood: a human experimental study. *Psychoneuroendocrinology* 2019;**109**:104371.

51. Kaiser H, Yu K, Pandya C. *et al.* Kynurenine, a tryptophan metabolite that increases with age, induces muscle atrophy and lipid peroxidation. *Oxidative Med Cell Longev* 2019;**2019**:9894238.

52. Westbrook R, Chung T, Lovett J. *et al.* Kynurenines link chronic inflammation to functional decline and physical frailty. *JCI Insight* 2020;**5**:e136091.

53. Gouasmi R, Ferraro-Peyret C, Nancey S. *et al.* The kynurenine pathway and cancer: why keep it simple when you can make it complicated. *Cancers (Basel)* 2022;**14**:2793.

54. Ballmann C, Tang Y, Bush Z. *et al.* Adult expression of PGC-$1\alpha$ and -$1\beta$ in skeletal muscle is not required for endurance exercise-induced enhancement of exercise capacity. *Am J Physiol Endocrinol Metab* 2016;**311**:E928–38.

55. Bartolomucci A, Pederzani T, Sacerdote P. *et al.* Behavioral and physiological characterization of male mice under chronic psychosocial stress. *Psychoneuroendocrinology* 2004;**29**: 899–910.

56. Stan TL, Vijver DVD, Verhaart IEC. *et al.* The vitamin B3 analogue nicotinamide riboside has only very minor effects on reducing muscle damage in mdx mice. 2023; *bioRxiv*, 2023.02.02.526793. https://www.biorxiv.org/content/10.1101/2023.02.02.526793v2.

57. Thereza M, Barbosa P, Soares SM. *et al.* The enzyme CD38 (a NAD glycohydrolase, EC 3.2.2.5) is necessary for the development of diet-induced obesity. *FASEB J* 2007;**21**:3629–39.

58. Guedes AGP, Deshpande DA, Dileepan M. *et al.* CD38 and airway hyper-responsiveness: studies on human airway smooth muscle cells and mouse models. *Can J Physiol Pharmacol* 2014;**93**: 145–53.

59. Camacho-Pereira J, Tarragó MG, Chini CCS. *et al.* CD38 dictates age-related NAD decline and mitochondrial dysfunction through an SIRT3-dependent mechanism. *Cell Metab* 2016;**23**: 1127–39.

60. Belanto JJ, Olthoff JT, Mader TL. *et al.* Independent variability of microtubule perturbations associated with dystrophinopathy. *Hum Mol Genet* 2016;**25**:4951–61.

61. Tinsley J, Deconinck N, Fisher R. *et al.* Expression of full-length utrophin prevents muscular dystrophy in mdx mice. *Nat Med* 1998;**4**:1441–4.

62. Baban B, Chandler P, McCool D. *et al.* Indoleamine 2,3-dioxygenase expression is restricted to fetal trophoblast giant cells during murine gestation and is maternal genome specific. *J Reprod Immunol* 2004;**61**:67–77.

63. Gulcev M, Reilly C, Griffin TJ. *et al.* Tryptophan catabolism in acute exacerbations of chronic obstructive pulmonary disease. *Int J COPD* 2016;**11**:2435–46.

64. Kanamori KS, de Oliveira GC, Auxiliadora-Martins M. *et al.* Two different methods of quantification of oxidized nicotinamide adenine dinucleotide (NAD+) and reduced nicotinamide adenine dinucleotide (NADH) intracellular levels: enzymatic coupled cycling assay and ultra-performance liquid chromatography (UPLC)-mass spectrometry. *Bio Protoc* 2018;**8**: e2937.